



HAL
open science

CaMK1D signaling in AgRP neurons promotes ghrelin-mediated food intake

Kevin Vivot, Gergö Meszaros, Zhirong Zhang, Eric Erbs, Gagik Yeghiazaryan, Erwan Grandgirard, Anna Schneider, Etienne Clauss-Creusot, Alexandre Charlet, Maya Faour, et al.

► **To cite this version:**

Kevin Vivot, Gergö Meszaros, Zhirong Zhang, Eric Erbs, Gagik Yeghiazaryan, et al.. CaMK1D signaling in AgRP neurons promotes ghrelin-mediated food intake. 2022. hal-03861746

HAL Id: hal-03861746

<https://hal.science/hal-03861746>

Preprint submitted on 20 Nov 2022

HAL is a multi-disciplinary open access archive for the deposit and dissemination of scientific research documents, whether they are published or not. The documents may come from teaching and research institutions in France or abroad, or from public or private research centers.

L'archive ouverte pluridisciplinaire **HAL**, est destinée au dépôt et à la diffusion de documents scientifiques de niveau recherche, publiés ou non, émanant des établissements d'enseignement et de recherche français ou étrangers, des laboratoires publics ou privés.

1 **CaMK1D signaling in AgRP neurons promotes ghrelin-mediated food intake**

2

3 Kevin Vivot^{1,2,3,4}, Gergö Meszaros^{1,2,3,4}, Zhirong Zhang^{1,2,3,4}, Eric Erbs^{1,2,3,4}, Gagik
4 Yeghiazaryan⁵, Mar Quiñones^{6,7}, Erwan Grandgirard^{1,2,3,4}, Anna Schneider^{1,2,3,4}, Etienne
5 Clauss--Creusot^{4,8}, Alexandre Charlet^{4,8}, Maya Faour⁹, Claire Martin⁹, Serge Luquet⁹, Peter
6 Kloppenburg⁵, Ruben Nogueiras^{6,7}, and Romeo Ricci^{1,2,3,4,10}

7

8

9 ¹Institut de Génétique et de Biologie Moléculaire et Cellulaire, Illkirch 67404, France

10 ²Centre National de la Recherche Scientifique, UMR7104, Illkirch 67404, France

11 ³Institut National de la Santé et de la Recherche Médicale, U964, Illkirch 67404, France

12 ⁴Université de Strasbourg, Strasbourg 67081, France

13 ⁵Biocenter, Institute for Zoology, and Cologne Excellence Cluster on Cellular Stress Responses
14 in Aging-Associated Diseases (CECAD), University of Cologne, Cologne 50674, Germany

15 ⁶Department of Physiology, CIMUS, University of Santiago de Compostela-Instituto de
16 Investigación Sanitaria, Santiago de Compostela 15782, Spain

17 ⁷CIBER Fisiopatología de la Obesidad y Nutrición (CIBERObn), Santiago de Compostela
18 15706, Spain

19 ⁸Centre National de la Recherche Scientifique, Institute of Cellular and Integrative
20 Neurosciences, Strasbourg 67084, France

21 ⁹Université de Paris, CNRS, Unité de Biologie Fonctionnelle et Adaptative, F-75013 Paris,
22 France.

23 ¹⁰Laboratoire de Biochimie et de Biologie Moléculaire, Nouvel Hôpital Civil, Strasbourg
24 67091, France

25 Correspondance: romeo.ricci@igbmc.fr

26

27 **Highlights**

- 28 • Whole-body deletion of *CaMK1D* in mice reduces food intake, ghrelin sensitivity and
29 protects against obesity.
- 30 • AgRP/NPY neuron-specific deletion of *CaMK1D* reduces food intake, ghrelin
31 sensitivity, energy expenditure and protects against obesity.
- 32 • CaMK1D is dispensable for ghrelin-stimulated electrical activity of AgRP neurons and
33 hypothalamic AMPK signaling.
- 34 • CaMK1D controls phosphorylation of CREB and CREB-dependent expression of the
35 orexigenic neuropeptides AgRP and NPY.

36

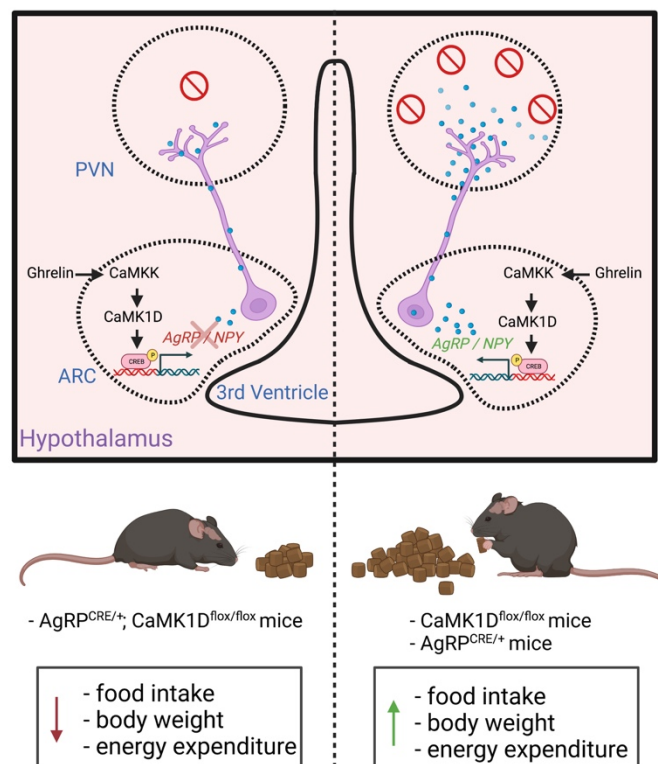
37 **Summary**

38 Hypothalamic AgRP/NPY neurons are key players in the control of feeding behavior. Ghrelin,
39 a major hormone released under fasting conditions, activates orexigenic AgRP/NPY neurons
40 to stimulate food intake and adiposity. However, cell-autonomous ghrelin-dependent signaling
41 mechanisms in AgRP/NPY neurons remain poorly defined. Here we demonstrate that
42 calcium/calmodulin-dependent protein kinase ID (CaMK1D), a genetic hot spot in type 2
43 diabetes, is activated in hypothalamus upon ghrelin stimulation and acts in AgRP neurons to
44 promote ghrelin-dependent food intake. Global *CaMK1D* knockout mice are resistant to the
45 orexigenic action of ghrelin, gain less body weight and are protected against high-fat diet-
46 induced obesity. Deletion of *CaMK1D* in AgRP but not in POMC neurons is sufficient to
47 recapitulate above phenotypes. Lack of CaMK1D attenuates phosphorylation of CREB and
48 CREB-dependent expression of the orexigenic neuropeptides AgRP/NPY as well as the

49 amount of AgRP fiber projections to the Paraventricular nucleus (PVN), while electrical
50 activity of AgRP neurons and 5' AMP-activated protein kinase (AMPK) signaling are
51 unaffected. Hence, CaMK1D links ghrelin action to transcriptional control of orexigenic
52 neuropeptide availability in AgRP neurons.

53

54 Graphical Abstract



55

56 Keywords

57 Obesity; Food intake regulation; AgRP neurons; ghrelin signaling; CaMK1D; CREB
58 phosphorylation; AgRP/NPY expression

59

60

61 **Introduction**

62 Tight regulation of energy homeostasis at multiple levels is instrumental for organisms to cope
63 with changes in food availability. The Central Nervous System (CNS) orchestrates a complex
64 array of processes mediating energy intake and expenditure. Hormonal, neuronal and
65 nutritional signals according to changes in food absorption, energy storage and energy
66 consumption in different organs reach the CNS which in turn triggers corresponding changes
67 in feeding behavior and peripheral cellular metabolism (Kim et al., 2018).

68 Sensing of the nutrient status of the organism is governed by distinct neuronal cell populations,
69 particularly within the arcuate nucleus (ARC) of the hypothalamus (Jais and Brüning, 2021).
70 Neurons in this region provide specific projections to other hypothalamic nuclei including the
71 paraventricular nucleus of the hypothalamus (PVN) or to different extrahypothalamic brain
72 regions that in turn coordinate corresponding behavioral responses (Morton et al., 2006).
73 Conversely, hypothalamic nuclei receive inputs from extrahypothalamic brain regions to
74 control food intake and energy expenditure (Waterson and Horvath, 2015). Hypothalamic
75 neurons also obtain signals from the mesolimbic reward system governing “hedonic” aspects
76 of food intake (Stuber and Wise, 2016).

77 Orexigenic neuropeptide Y (NPY) and agouti-related peptide (AgRP)-expressing AgRP/NPY
78 neurons and anorexigenic proopiomelanocortin (POMC)-expressing neurons in the arcuate
79 nucleus of the hypothalamus are primarily involved in the regulation of energy homeostasis.
80 To control appetite and peripheral metabolism, these neurons are regulated by several
81 hormones. Among others, leptin, ghrelin and insulin emerged as key players in this context.
82 Both leptin and insulin receptors are expressed in these neurons and both insulin and leptin
83 have been found to activate POMC and to inhibit AgRP/NPY neurons (Timper and Brüning,
84 2017). Ghrelin enhances the activity of AgRP/NPY neurons via its receptors, while it decreases

85 the action of POMC neurons through a ghrelin receptor-independent mechanism (Chen et al.,
86 2017).

87 Dysfunction of these neuronal circuits is known to contribute to overnutrition and obesity that
88 eventually culminates in metabolic disorders such as type 2 diabetes (T2D) and/or
89 cardiovascular diseases. Obesity and T2D are interlinked and complex metabolic disorders.
90 Recent Genome-wide association studies (GWAS) and GWAS meta-analyses revealed
91 complex polygenic factors influencing the development of both diseases. In fact more than
92 ~250 genetic loci have been identified for monogenic, syndromic, or common forms of T2D
93 and/or obesity-related traits (Bonnetfond and Froguel, 2015; Locke et al., 2015). Despite these
94 remarkable advancements, the contribution of most obesity- and T2D-associated single
95 nucleotide polymorphism (SNPs) to the pathogenesis of these diseases remains largely elusive.
96 CDC123 (cell division cycle protein 123)/CaMK1D (calcium/calmodulin-dependent protein
97 kinase ID) represents one such locus on chromosome 10, strongly associated with T2D in
98 European and Asian populations (Kooner et al., 2011; Shu et al., 2010; Zeggini et al., 2008).
99 Among other variants, fine mapping identified rs11257655 as the predominant SNP within this
100 locus (Morris et al., 2012). The change from C to T in the enhancer region of the rs11257655
101 allele, promotes DNA hypomethylation and the binding of the transcription factors
102 FOXA1/FOXA2 on the enhancer region resulting in enhanced CaMK1D gene transcription
103 (Turner et al., 2018; Xue et al., 2018). Thus, CaMK1D expression might be enhanced and
104 contributes to the development of T2D.

105 CaMK1D (or CaMK1 δ) is the fourth member of the CaMK1 subfamily. CAMK1 has been
106 described to be ubiquitously expressed at low levels in most tissues. Importantly however,
107 CAMKI proteins are highly expressed in several brain regions, including the cortex,
108 hippocampus, thalamus, hypothalamus, midbrain, and olfactory bulb, with each isoform
109 exhibiting distinct spatiotemporal expression during neuronal development (Kamata et al.,

110 2007). Ca²⁺/Calmodulin (CaM) binding and subsequent phosphorylation at Thr180 by CaMKK
111 are required for CaMKI activation. In the particular case of CaMK1D, the phosphorylation of
112 CaMK1D by CaMKK, induces a resistance to protein phosphatases, which keeps CaMK1D in
113 a 'primed' state, to facilitate its activation in response to Ca²⁺ signals (Senga et al., 2015).

114 CaMKIs have been mainly shown to be important in neurons. CaMKIs control neuron
115 morphology (Buchser et al., 2010) including axonal extension, growth cone motility (Wayman
116 et al., 2004) and dendritogenesis (Takemoto-Kimura et al., 2007). It has been demonstrated
117 that CaMKIs may also regulate neuronal function by controlling the long-term potentiation, a
118 process involving persistent strengthening of synapses that leads to a long-lasting increase in
119 signal transmission between neurons (Schmitt et al., 2005). However, specific non-redundant
120 neuronal functions of any of the four members of the CaMKI subfamily including CaMK1D
121 have yet to be determined. In fact, CaMK1D has been shown to be implicated in neutrophil
122 function (Verploegen et al., 2005). The genetic association of the *CaMK1D* locus with T2D
123 and correlation of clinical data revealed that CaMK1D might promote pancreatic β cell
124 dysfunction (Simonis-Bik et al., 2010). However, direct experimental evidence for the latter
125 conclusion is lacking thus far. Another study proposed that CaMK1D stimulates hepatic
126 glucose output, a mechanism contributing to T2D (Haney et al., 2013).

127 Using global and conditional CaMK1D knockout mice, we provide evidence for a role of
128 CaMK1D in central regulation of food intake, while its function seems to be redundant in the
129 liver and in the pancreatic β cell. We demonstrate that CaMK1D acts in hypothalamic AgRP
130 neurons to control food intake in response to ghrelin. While CaMK1D in AgRP neurons is
131 redundant for ghrelin-stimulated increase in electrical neuronal activity and AMPK signaling,
132 its absence impairs ghrelin-induced activatory CREB phosphorylation, AgRP transcription and
133 AgRP/NPY fiber abundance within the PVN. Our data thus unveil ghrelin signaling

134 mechanisms in AgRP neurons downstream or independent of neuronal activation to be
135 necessary for efficient appetite stimulation.

136

137 **Results**

138 **Global deletion of CaMK1D in mice protects against obesity**

139 To understand the function of CaMK1D in metabolism, we generated mice carrying a floxed
140 allele of *CaMK1D* (Figure S1A) and crossed them with the global Cre-deleter, Rosa26-Cre
141 (Soriano, 1999), to obtain whole-body knockout mice. Western blotting confirmed efficient
142 deletion of CaMK1D in different organs including brain, pancreas and intestine (Figure 1A).
143 Whole-body *CaMK1D* knockout mice (*CaMK1D*^{-/-} mice) were born in expected gender
144 distribution (Figure S1B) and Mendelian ratios (Figure S1C) and developed without overt
145 problems. Body and tibia lengths at 7 weeks of age were equal in *CaMK1D*^{-/-} and *CaMK1D*
146 *WT* mice (*CaMK1D*^{+/+} mice) (Figure S1D and S1E), thus excluding any major postnatal growth
147 defect. However, body weight gain in *CaMK1D*^{-/-} mice on a chow diet was significantly
148 reduced from 16 weeks on after starting to measure weight at the age of 5 weeks as compared
149 to *CaMK1D*^{+/+} mice. This significant difference was exacerbated when obesity was induced in
150 mice on a high fat diet (HFD) at the age of 5 weeks (Figure 1B). Quantitative Nuclear Magnetic
151 Resonance (qNMR) revealed that HFD-fed *CaMK1D*^{-/-} mice compared to *CaMK1D*^{+/+} mice
152 had a reduced fat mass, while there was no significant difference in the lean mass and free body
153 fluid (FBF) (Figure 1C). In line with reduced obesity, fasted glucose levels at 10 weeks after
154 HFD feeding in *CaMK1D*^{-/-} mice was significantly reduced as compared to *CaMK1D*^{+/+} mice
155 (Figure 1D). In fact, glucose levels in *CaMK1D*^{-/-} mice on a HFD were similar as in
156 corresponding chow diet-fed mice indicating that they were protected from obesity-induced
157 hyperglycemia. There was no apparent difference in fasting glucose levels between *CaMK1D*^{-/-}

158 $^{-/-}$ and $CaMK1D^{+/+}$ mice on a chow diet (Figure 1D). The observed reduced fasting glucose
159 levels correlated with reduced fasting insulin levels (Figure 1E). Glucose tolerance was
160 slightly, but not significantly, improved in $CaMK1D^{-/-}$ as compared to $CaMK1D^{+/+}$ mice on a
161 chow diet (Figure 1F). However, these differences became significant in mice on a HFD
162 (Figure 1G and 1H). While insulin sensitivity was unaltered in $CaMK1D^{-/-}$ mice on a chow diet
163 (Figure 1I), it was significantly improved in $CaMK1D^{-/-}$ as compared to $CaMK1D^{+/+}$ mice on
164 a HFD (Figure 1J and 1K). Glucose-induced secretion of insulin (GSIS) was slightly but not
165 significantly reduced in $CaMK1D^{-/-}$ mice as compared to $CaMK1D^{+/+}$ mice on a HFD (Figure
166 S2A). GSIS from isolated islets of $CaMK1D^{-/-}$ and $CaMK1D^{+/+}$ mice was comparable (Figure
167 S2B).

168 To further exclude a primary role of CaMK1D in the pancreas including β cells, we crossed
169 floxed mice with $PDX1^{Cre/+}$ mice (Gu et al., 2002). Western blotting confirmed that deletion of
170 $CaMK1D$ in the pancreas was efficient, while no apparent deletion was visible in brain (Figure
171 S2C) or other organs (data not shown). Pancreas-specific $CaMK1D$ knockout mice
172 ($PDX1^{Cre/+};CaMK1D^{lox/lox}$ mice) did not show any differences in body weight gain and
173 glucose tolerance as compared to floxed control mice ($CaMK1D^{lox/lox}$ mice) on a chow diet as
174 well as HFD (Figure S2D-F), confirming that CaMK1D is redundant in β cell function.

175 Hepatic insulin resistance leading to increased gluconeogenesis is an important mechanism
176 contributing to obesity-related changes in glucose homeostasis. Therefore, we generated liver-
177 specific knockout mice using $Albumin^{Cre/+}$ mice (Postic et al., 1999) ($Alb^{Cre/+};CaMK1D^{lox/lox}$
178 mice) and corresponding floxed control mice ($CaMK1D^{lox/lox}$ mice). Quantitative reverse
179 transcription PCR (qRT-PCR) confirmed efficient deletion of CaMK1D in the liver (Figure
180 S2G) but not in other organs (data not shown). However, hepatic deletion of $CaMK1D$ did not
181 affect body weight gain, glucose tolerance and insulin sensitivity in mice on a chow diet as

182 well as on HFD (Figure S2H-L). Thus, our data exclude any major functions of CaMK1D in
183 pancreatic β cells and liver under both normal and obesity conditions.

184

185 **Global deletion of CaMK1D alters ghrelin-mediated food intake**

186 To further understand reduced body weight gain and fat mass in *CaMK1D*^{-/-} mice as compared
187 to *CaMK1D*^{+/+} mice, we next explored energy metabolism. In line with reduced obesity,
188 cumulative food intake was decreased in *CaMK1D*^{-/-} mice as compared to *CaMK1D*^{+/+} mice
189 on a chow diet as well as on HFD reaching significance at 16 weeks after starting to measure
190 it (Figure 2A). Likewise, cumulative food intake in response to 24 hours fasting was
191 significantly reduced in *CaMK1D*^{-/-} mice throughout the observed period of refeeding as
192 compared to *CaMK1D*^{+/+} mice (Figure 2B). Indirect calorimetry revealed that energy
193 expenditure (Figure 2C and 2D), O₂ consumption (Figure 2E) CO₂ production (Figure 2F) and
194 the respiration exchange rate (RER) (Figure 2G) were equal in *CaMK1D*^{-/-} mice as compared
195 to *CaMK1D*^{+/+} mice on a HFD. Moreover, the locomotor activity under basal conditions was
196 comparable in *CaMK1D*^{-/-} mice and *CaMK1D*^{+/+} mice (data not shown). However, locomotor
197 activity of *CaMK1D*^{-/-} as compared to *CaMK1D*^{+/+} mice was significantly reduced in the night
198 period after 24 hours fasting (Figure 2H and 2I) in line with reduced appetite and reduced
199 seeking for food in response to fasting. Thus, reduced obesity primarily correlated with reduced
200 appetite and food intake.

201 Ghrelin is a gut-derived hormone released in response to fasting and promotes feeding behavior
202 and adiposity (Müller et al., 2015). Given that the resistance to diet-induced obesity of
203 *CaMK1D*^{-/-} mice could be explained by reduced food intake, we next wondered whether the
204 ghrelin response was affected in mice lacking *CaMK1D*. To this end, we determined
205 cumulative food intake upon intraperitoneal injections of ghrelin in mice on a chow diet. While

206 *CaMK1D*^{+/+} mice showed a significant increase in cumulative food intake at 4 and 6 hours
207 after ghrelin injections, such a response was almost absent in *CaMK1D*^{-/-} mice (Figure 2J). In
208 contrast, the response to leptin was comparable in *CaMK1D*^{+/+} mice and *CaMK1D*^{-/-} mice
209 (Figure 2K). Blood levels of acylated ghrelin were significantly higher in *CaMK1D*^{-/-} as
210 compared to *CaMK1D*^{+/+} mice on a HFD (Figure 2L) in line with an adaptive response to a
211 primary defect in ghrelin action. Conversely, blood levels of leptin were significantly lower in
212 *CaMK1D*^{-/-} mice as compared to *CaMK1D*^{+/+} mice (Figure 2M) on a HFD, correlating well
213 with the degree of obesity.

214 To exclude any major anxiety-like behavior or stress-induced anhedonia, we subjected mice to
215 an open field and to a sucrose preference test, respectively. No major differences between
216 genotypes could be observed (Figure S3A-H). Thus, lack of *CaMK1D* results in a compromised
217 ghrelin response, which is in line with reduced obesity.

218

219 **CaMK1D acts in AgRP neurons to regulate food intake in response to ghrelin**

220 Ghrelin stimulates central neurons to promote feeding. We thus next asked whether CaMK1D
221 in the nervous system was mainly responsible for the observed phenotype in *CaMK1D*^{-/-} mice.
222 We therefore crossed *CaMK1D*^{fllox/fllox} mice with *Nestin*^{Cre/+} mice resulting in efficient deletion
223 of *CaMK1D* in brain including hypothalamus but not in other organs such as intestine and
224 pancreas (Figure S4A). Indeed, the body weight gain was significantly attenuated in nervous
225 system-specific *CaMK1D* knockout mice (*Nestin*^{Cre/+}; *CaMK1D*^{fllox/fllox} mice) as compared to
226 Cre and floxed control mice (*Nestin*^{Cre/+} mice and *CaMK1D*^{fllox/fllox} mice) on a chow diet as well
227 as on HFD (Figure S4B). Cumulative food intake was decreased in *Nestin*^{Cre/+}; *CaMK1D*^{fllox/fllox}
228 mice as compared to control mice on a chow diet (Figure S4C) as well as on a HFD (Figure
229 S4D). Likewise, cumulative food intake in response to 24 hours fasting was significantly

230 reduced in *Nestin^{Cre/+};CaMK1D^{lox/lox}* mice as compared to control mice after 4, 14 and 24
231 hours of refeeding (Figure S4E). Consistently, while control mice showed a significant increase
232 in cumulative food intake at 4 and 6 hours after ghrelin injections, such a response was absent
233 in *Nestin^{Cre/+};CaMK1D^{lox/lox}* mice (Figure S4F).

234 Ghrelin primarily acts on hypothalamic neurons in the arcuate nucleus. In particular, it
235 stimulates NPY/AgRP neurons to promote appetite (Andrews et al., 2008). Given our results
236 in nervous system-specific knockout mice, we next asked whether CaMK1D acts in AgRP
237 neurons to control food intake. To this end, we crossed *CaMK1D^{lox/lox}* mice with *AgRP^{Cre/+}*
238 mice resulting in efficient recombination of the *CaMK1D* locus in hypothalamus but not in the
239 brain cortex, liver, tail and white blood cells (Figure 3A). Strikingly, AgRP neuron-specific
240 knockout mice (*AgRP^{Cre/+}; CaMK1D^{lox/lox}* mice) gained significantly less weight as compared
241 to Cre and floxed control mice (*AgRP^{Cre/+}* mice and *CaMK1D^{lox/lox}* mice) on a chow diet as
242 well as on HFD (Figure 3B). Similar to nervous system-specific knockout mice, *AgRP^{Cre/+}*;
243 *CaMK1D^{lox/lox}* mice showed significantly less cumulative food intake as compared to control
244 mice on a chow diet (Figure 3C) as well as HFD (Figure 3D). Similar significant differences
245 were observed in the cumulative food intake in response to 24 hours fasting (Figure 3E) as well
246 as in response to ghrelin injection (Figure 3F). Importantly, no such differences could be
247 detected when deleting *CaMK1D* in anorexigenic POMC neurons (Figure S5A–F), suggesting
248 that the effects of CaMK1D on food intake are specific to AgRP neurons.

249 To further evaluate a role of CaMK1D in AgRP neuron-dependent energy metabolism, we next
250 performed indirect calorimetry with *AgRP^{Cre/+};CaMK1D^{lox/lox}* mice and control mice on a
251 chow diet. Cumulative food intake (Figure 4A) and locomotor activity (Figure 4B and 4C)
252 were comparable in *CaMK1D^{-/-}* mice and *CaMK1D^{+/+}* mice. Interestingly, energy expenditure
253 (Figure 4D and 4E) was decreased in *AgRP^{Cre/+};CaMK1D^{lox/lox}* mice as compared to control
254 mice. The regression-based analysis-of-covariance (ANCOVA) confirmed that there was a

255 body weight-independent metabolic rate (MR) difference with lower MR in the
256 *AgRP^{Cre/+};CaMK1D^{lox/lox}* relative to the control mice (Figure 4F). In line with these findings,
257 O₂ consumption (Figure 4G) and CO₂ production (Figure 4H) were also reduced, while the
258 respiration exchange rate (RER) (Figure 4I) was equal. Given the overall reduction in body
259 weight gain, reduced energy expenditure was most likely compensatory to compromised
260 energy availability caused by reduced food intake. Altogether, our data thus suggest that
261 CaMK1D acts in AgRP neurons to primarily control food intake in response to ghrelin.

262

263 **Deletion of CaMK1D in mice does not affect AgRP/NPY neuronal activity in response to**
264 **ghrelin.**

265 c-fos expression is used as a marker for neuronal activity (Hoffman et al., 1993). To understand
266 the function of CaMK1D in ghrelin-induced neuronal activity, we next explored c-fos
267 expression in AgRP neurons in the absence and presence of CaMK1D. Immunofluorescence
268 of c-fos revealed no significant differences in basal and ghrelin-induced expression of c-fos in
269 ARC neurons of *CaMK1D^{-/-}* mice as compared to control mice on a chow diet (Figure 5A and
270 5B). To verify this finding, we compared the effect of ghrelin on AgRP neurons between both
271 mice lines using perforated patch clamp recordings in brain slices. To identify AgRP neurons,
272 we generated *CaMK1D^{-/-}* and *CaMK1D^{+/+}* mice carrying a EGFP reporter under the control of
273 the *AgRP* promoter (*CaMK1D^{-/-}-AgRP-EGFP* and *CaMK1D^{+/+}-AgRP-EGFP* mice) (Figure
274 5C). The ghrelin-induced increases in action potential frequency were similar in AgRP neurons
275 of *CaMK1D^{-/-}-AgRP-EGFP* as compared to *CaMK1D^{+/+}-AgRP-EGFP* mice (*CaMK1D^{+/+}*,
276 n=12; *CaMK1D^{-/-}*, n=10, p=0.82) (Figure 5D and 5E). Between the two mouse lines, we also
277 found no significant differences in general intrinsic electrophysiological properties of AgRP
278 neurons such as spontaneous actions potential frequency, input resistance, excitability, and

279 whole-cell capacitance (Figure 5F-I). Taken together, these data suggest that CaMK1D is
280 redundant for ghrelin-stimulated activation of AgRP neurons.

281

282 **Ghrelin activates CaMK1D to induce AgRP/NPY expression and projections in the PVN**

283 Lack of CaMK1D did not affect ghrelin-induced increase in electrical activity of AgRP neurons
284 prompting us to hypothesize that CaMK1D acts downstream or independent of neuronal
285 activity. We thus next asked whether CaMK1D is activated upon ghrelin. We first used Phos-
286 tag gels to address CaMK1D phosphorylation in response to ghrelin in cultured primary
287 hypothalamic cells isolated from *CaMK1D*^{-/-} and *CaMK1D*^{+/+} mice. Indeed, phosphorylated
288 CaMK1D as marked by the upshifted detected band increased upon ghrelin stimulation (Figure
289 6A). Calcium/calmodulin directly activates calcium/calmodulin-dependent protein kinase I by
290 binding to the enzyme and indirectly promotes the phosphorylation and synergistic activation
291 of the enzyme by calcium/calmodulin-dependent protein kinase kinase (CaMKK) (Haribabu et
292 al., 1995). In line with above findings in cultured neurons, activatory phosphorylation of
293 CaMK1D increased in hypothalamus of ghrelin-stimulated *CaMK1D*^{+/+} mice, while no
294 phosphorylation of CaMK1D or total protein was visible in *CaMK1D*^{-/-} samples (Figure 6B).

295 Ghrelin stimulates AMPK activity in the hypothalamus (Andersson et al., 2004). However,
296 ghrelin-induced AMPK activity was equal in primary hypothalamic neurons of *CaMK1D*^{-/-} and
297 *CaMK1D*^{+/+} mice as shown by assessment of activatory phosphorylation of AMPK and
298 phosphorylation of its target acetyl-CoA carboxylase (ACC) (Figure 6C). Ghrelin-induced
299 cAMP response element (CRE)-binding protein (CREB) phosphorylation promotes expression
300 of AgRP and NPY that mediate the orexigenic action of ghrelin (Sakkou et al., 2007).
301 Interestingly, despite higher basal expression of total CREB, levels of phosphorylated CREB
302 were lower in control treated as well as ghrelin-treated *CaMK1D*^{-/-} cells as compared to

303 *CaMK1D*^{+/+} cells (Figure 6C). Even though activatory phosphorylation of CREB was induced
304 upon ghrelin stimulation in *CaMK1D*^{-/-} cells, ghrelin-induced transcription of AgRP and NPY
305 but not POMC was almost abolished in *CaMK1D*^{-/-} cells (Figure 6D), indicating that the overall
306 reduction of activatory CREB phosphorylation constitutes at least one plausible explanation
307 for reduced CREB-dependent expression of AgRP and NPY. In addition, AgRP
308 immunohistochemistry revealed reduced levels of this neuropeptide in synaptic projections of AgRP
309 neurons located in the PVN of *CaMK1D*^{-/-} mice under stimulatory conditions as compared to
310 control animals (Figure 6E and F). Reduced levels and thus decreased inhibitory action of
311 AgRP and NPY on predominantly anorexigenic neurons in the PVN is thus a likely mechanism
312 underlying reduced food intake and body weight gain despite normal AgRP neuronal activity.
313 Hence, CaMK1D in AgRP neurons is required for CREB-dependent expression of the
314 orexigenic neuropeptides AgRP and NPY, thereby regulating food intake and obesity.

315

316

317 **Discussion**

318 A possible role of CaMK1D in obesity and T2D has been predicted based on recent GWAS
319 studies. However, the function of CaMK1D in physiology and metabolic disease *in vivo* was
320 unknown thus far. In our study, using a loss-of-function approach in mice, we discovered an
321 unpredicted role of CaMK1D in central control of food intake. We also excluded a cell-
322 autonomous role of CaMK1D in the liver and pancreas to maintain energy homeostasis.

323 We found that CaMK1D is specifically required in AgRP neurons to promote ghrelin- induced
324 hyperphagia and body weight gain. As genetic studies predicted enhanced expression of
325 CaMK1D to contribute to T2D (Thurner et al., 2018; Xue et al., 2018), our data also fit with a
326 model in which enhanced CaMK1D signaling in AgRP neurons promotes obesity. Deletion of
327 *CaMK1D* in AgRP neurons is sufficient to trigger significant effects on body weight and food
328 intake seen in global *CaMK1D* knockout mice highlighting the importance of CaMK1D
329 signaling in this subpopulation of neurons. In line with this, CaMK1D is activated by ghrelin
330 in NPY/AgRP neurons. Yet, we cannot fully exclude other central functions of CaMK1D
331 signaling that may also contribute to altered body weight gain. Given the fact that AgRP neuron
332 activity has been linked to control of liver glucose production and insulin sensitivity (Könner
333 et al., 2007) as well as nutrient partitioning through dynamic change of the autonomic nervous
334 system (Denis et al., 2014), it is still possible that lack of CaMK1D specifically in AgRP neuron
335 alters insulin and glucose metabolism in addition of the feeding phenotype. Moreover,
336 CaMK1D is widely expressed in the CNS and ghrelin has been reported to act in different
337 hypothalamic and extrahypothalamic areas to induce feeding. Having that said, we showed that
338 CaMK1D is redundant in anorexigenic POMC neurons. Even though deletion of *CaMK1D* in
339 AgRP neurons largely recapitulates phenotypes seen in whole-body knockout mice, this does
340 not fully exclude functions in other organs implicated in energy homeostasis that we did not
341 yet explore.

342 Importantly, CaMK1D is dispensable for ghrelin-stimulated electrical activity of AgRP
343 neurons. This finding is in line with a model in which ghrelin-driven neuronal activity induces
344 membrane depolarization and calcium changes which in turn may trigger CaMK1D activation
345 and CaMK1D-dependent responses including CREB-dependent transcription (Sheng et al.,
346 1991). Thus, our study has identified a so far unknown signaling pathway in AgRP neurons
347 that links neuronal activity to CREB-dependent transcription (Figure 6G).

348 CREB-dependent transcription has been shown to regulate fundamental processes in neuronal
349 development, activity-dependent dendritic outgrowth, and synaptic plasticity (Flavell and
350 Greenberg, 2008). In AgRP neurons, CREB controls transcription of AgRP and NPY (Sakkou
351 et al., 2007). In accordance with this finding, we found that ghrelin failed to induce AgRP and
352 NPY transcription in *CaMK1D*-deficient hypothalamus and that the number of AgRP
353 projections to the PVN were reduced. In fact, it has been demonstrated that ghrelin failed to
354 stimulate feeding upon chemical and genetic inhibition of AgRP and NPY (Andrews et al.,
355 2008; Aponte et al., 2011; Chen et al., 2004; Luquet et al., 2005; Nakazato et al., 2001). Even
356 though AgRP is one of the crucial neuropeptides inhibiting anorexigenic neurons in the PVN,
357 other CREB-dependent functions might be affected in *CaMK1D*-deficient AgRP neurons that
358 may also contribute to the observed metabolic phenotypes to be investigated in the future.
359 Moreover, CaMK1D might also regulate CREB-independent functions that need to be
360 identified.

361 Central ghrelin administration induced AMPK phosphorylation and activation (Kola et al.,
362 2005; López et al., 2008) and ghrelin responses could be alleviated through AMPK inhibition
363 (Anderson et al., 2008). AMPK activation was dependent on calcium changes and on CaMKK
364 2 activation (Anderson et al., 2008). CaMKK is also known to activate CaMK1 including
365 CaMK1D (Figure 6G). Interestingly, AMPK activation was shown to occur in the ventro-
366 medial nucleus of the hypothalamus (VMH), since adenoviral delivery of a dominant negative

367 isoform of AMPK into the VMH was sufficient to block ghrelin-induced food intake (Anderson
368 et al., 2008; García et al., 2001; López et al., 2008). Therefore, it has been suggested that
369 AgRP/NPY levels in neurons in the ARC are regulated at a presynaptic level by AMPK
370 signaling in neurons of the VMH. We found here that lack of CaMK1D almost entirely
371 abolished the increase in AgRP/NPY transcription in response to ghrelin. Yet, absence of
372 CaMK1D does not affect AMPK signaling in response to ghrelin in the hypothalamus. Given
373 that AgRP neuron-specific deletion of CaMK1D is sufficient to reduce food intake in response
374 to ghrelin, we propose that the transcriptional control of AgRP/NPY expression primarily
375 depends on CaMK1D signaling in AgRP neurons. Whether CaMK1D signaling occurs
376 downstream of AMPK-dependent presynaptic mechanisms remains to be explored. Another
377 possibility is that CaMK1D in AgRP neurons is required to integrate the trophic action of
378 ghrelin. Indeed, neural projections arising from AgRP neurons are fully established during a
379 critical window both during development and in the weeks around birth (Bouret et al., 2004).
380 Trophic action of ghrelin in that window of development has been show to control ARC AgRP
381 neurons PVN fibers growth and connection (Steculorum et al., 2015). Hence, one can
382 hypothesize that impaired transcriptional regulation of NPY and AgRP in AgRP neurons as a
383 consequence of CaMK1D deletion also led to developmental defects affecting post-natal
384 hypothalamic wiring and leading to altered metabolic control.

385 Elevated levels of cAMP led to CREB phosphorylation at serine 133 and mutation of this site
386 abrogated CREB-dependent reporter gene activation (Gonzalez and Montminy, 1989). Protein
387 kinase A (PKA) is a main mediator of cAMP-dependent phosphorylation of CREB. Indeed,
388 ghrelin was shown to increase calcium through the cAMP-PKA pathway in NPY-expressing
389 cells in the ARC of rats (Kohno et al., 2003). However, we observe that phosphorylation of
390 CREB depends, at least partially, on CaMK1D activity. In fact, CREB was shown to be
391 phosphorylated *in vitro* by both kinases, PKA and CaMK1 (Sheng et al., 1991). Given that

392 phosphorylation is reduced but not abolished in the absence of CaMK1D both kinases might
393 be necessary to exert robust CREB phosphorylation in response to ghrelin.

394 mTOR-S6K1 signaling has also been demonstrated to be involved in hypothalamic regulation
395 of food intake in response to ghrelin through regulation of CREB phosphorylation and
396 AgRP/NPY expression (Martins et al., 2012; Stevanovic et al., 2013). However, it is unclear
397 so far how and in which neurons mTOR-S6K1 regulates ghrelin responses. In fact, mTORC1
398 signaling in AgRP neurons was shown to control circadian expression of AgRP and NPY but
399 was redundant for regulation of food intake (Albert et al., 2015).

400 Altogether, we uncovered a signaling mechanism that acts in AgRP neurons to control levels
401 of AgRP and NPY, two main orexigenic neuropeptides centrally involved in promoting food
402 intake. Uncontrolled CaMK1D signaling in AgRP neurons represents thus a valuable
403 mechanism promoting obesity and T2D.

404

405

406

407 **Figure legends**

408 **Figure 1. Global Deletion of *CaMK1D* gene reduces obesity in mice.** (A) Expression of
409 CaMK1D protein in different tissues as indicated. Tissues from the wild type (*CaMK1D*^{+/+}) and
410 whole-body *CaMK1D* knockout (*CaMK1D*^{-/-}) mice were analyzed for CaMK1D expression by
411 western blot. (B) Body weight gain of mice with indicated genotypes fed with a Chow diet (CD)
412 or a High Fat Diet (HFD). (n=9 to 11/ group). (C) Body composition of mice with indicated
413 genotypes fed with a HFD measured by qNMR. (n=9/ group) (*p ≤ 0.05) (FBF = free body fluid).
414 (D) 4 hours fasted blood glucose levels at indicated time points. (n=8 to 10 / group). (E) 4 hours
415 fasted plasma insulin levels at indicated time points. (n=9 to 11 / group). (F-H) Blood glucose levels

416 during an IPGTT in mice with the indicated genotypes and diets. IPGTT was performed after an
417 overnight food withdrawal. Corresponding areas Under the Curve (AUC) are depicted. (n=9 to 12
418 / group). (I-K) Blood glucose levels during ITT in mice with the indicated genotypes and diets.
419 IPGTTs were performed after a 4H food withdrawal. kITTs obtained from ITT are depicted. (n=6
420 to 10 / group).

421 *p < 0.05 and **p < 0.01. Statistical tests included two-way ANOVA (B, H and J) and unpaired
422 Student's t test (C, D, E, H and K).

423

424 **Figure 2. Deletion of *CaMK1D* attenuates ghrelin-induced food intake.** (A) Cumulative food
425 intake from mice with indicated genotypes and diets. (n=9 to 11 / group). (B) Cumulative food
426 intake from mice with indicated genotypes on a HFD. Food intake was determined 24H after food
427 withdrawal. (n=12 to 17 / group). (C) Energy expenditure, (D) Regression-based analysis of
428 absolute MR against body mass. The ANCOVA analysis was done with MR as a dependent
429 variable, the genotype as a fixed variable and body mass as a covariate. (E) consumed O₂, (F)
430 produced CO₂ and (G) the respiratory exchange ratio (RER) in HFD fed control (*CaMK1D*^{+/+}) and
431 whole body *CaMK1D* knockout (*CaMK1D*^{-/-}) mice (n=9 / group). (H-I) Ambulatory activity over
432 24H. Ambulatory activity was measured with mice deprived from food for 24H. AUC from 5PM
433 to 11PM was calculated (n=6 / group). (J) Cumulative food intake after ghrelin injections (30 µg /
434 day) of mice with indicated genotypes on a chow diet. (n=6 to 7 / group). (K) Cumulative food
435 intake after leptin injections (3mg / kg) of mice with indicated genotypes on a chow diet. Food
436 intake was determined 24H after food withdrawal. (n=6 to 7 / group).

437 (L) Blood acylated Ghrelin and (M) Blood Leptin levels in mice with indicated genotypes on a
438 HFD. Blood sampling was performed 4H after food withdrawal. (N=5 to 8 / group).

439 *p < 0.05 and **p < 0.01. Statistical tests included two-way ANOVA (A, B), ANCOVA (D) and
440 unpaired Student's t test (I,J,K,L,M).

441 **Figure 3. Conditional deletion of *CaMK1D* in AgRP neurons leads to reduced body weight**

442 **gain and food intake.** (A) Verification of recombination in the *CaMK1D* locus in hypothalamus

443 (Hyp), cortex (Ctx), liver, tail and white blood cells (WBC) from mice with indicated genotypes.

444 DNA from tissues were analyzed by PCR with primers amplifying either recombined or floxed

445 alleles, respectively. (B) Body weight gain of mice with indicated genotypes on a Chow diet (CD)

446 or on a High Fat Diet (HFD). (n=10 to 15/ group).

447 (C-D) Cumulative food intake of mice with indicated genotypes fed on Chow diet or on high fat

448 diet. (n=10 to 15 / group). (E) Cumulative food intake of mice with indicated genotypes and diets.

449 Food intake was determined 24H after fasting. (n=12 to 17 / group). (F) Cumulative food intake

450 after ghrelin injections of mice with indicated genotypes and diets. (n=6 to 7 / group).

451 *p < 0.05, **p < 0.01 and ***p < 0.001. Statistical tests included two-way ANOVA (B,C,D) and

452 unpaired Student's t test (E, F).

453 **Figure 4. Conditional deletion of *CaMK1D* in AgRP neurons decreases energy expenditure.**

454 (A) Cumulative food intake from mice with indicated genotypes on a CD. Food intake was

455 determined 48H during indirect calorimetric measurements. (N=10 to 11 / group). (B-C)

456 Locomotor activity over 48H in mice with indicated genotypes on a Chow diet. (D-E) Energy

457 expenditure, (F) Regression-based analysis of absolute MR against body mass. The ANCOVA

458 analysis was done with MR as a dependent variable, the genotype as a fixed variable and body

459 mass as a covariate. (G) consumed O₂, (H) produced CO₂ and (I) the respiratory exchange ratio

460 (RER) in of mice with indicated genotypes on a Chow diet. All indirect calorimetric measurements

461 were done in automated cages. (N=10-11/ group).

462 *p < 0.05, **p < 0.01 and ***p < 0.001. Statistical tests included two-way ANOVA (A), ANCOVA

463 (F) and unpaired Student's t test (E,G,H).

464

465 **Figure 5. CaMK1D is dispensable for ghrelin-induced CaMK1D is dispensable for**
466 **ghrelin-induced electrophysiological activation of AgRP/NPY neurons**

467 (A-B) Representative immunofluorescence and quantification of c-fos⁺ cells in the ARC of mice
468 with indicated genotypes. Animals were injected with 30 µg ghrelin or vehicle and 2H after
469 injections whole hypothalamus was removed. (C) Recording situation shown in a brightfield
470 (top) and fluorescent image (bottom). The AgRP neuron expressed EGFP (green) and the
471 recording pipette contained tetramethyl rhodamine dextrane (red) to monitor membrane
472 integrity during the perforated patch clamp recording. (D) Recording of an AgRP neuron from
473 a *CaMK1D*^{+/+} mouse during ghrelin (100 nM) bath application. Top: Rate histogram, bin width:
474 10 s. Middle: Original recording. Bottom: Segments of the original recording in higher time
475 resolution. The numbers indicate the time points from which the segments originate. (E)
476 Ghrelin responses of AgRP neurons from *CaMK1D*^{+/+} and in *CaMK1D*^{-/-} mice, expressed as
477 change in action potential frequency. Top: Mean (± SEM) responses during the first 5 min of
478 ghrelin application. Bottom: Box plots showing the change in action potential frequency
479 measured between 6 and 8 min of ghrelin application. (F-I) Basic electrophysiological
480 properties of AgRP neurons in *CaMK1D*^{+/+} and in *CaMK1D*^{-/-} mice. (F) Spontaneous action
481 potential frequency. (G) Excitability assessed by the number of action potentials (APs) as a
482 function of current pulse (1s) amplitude. (H) Input resistance. (I) Whole-cell capacitance. The
483 horizontal lines in the box plots show the median. The whiskers were calculated according to
484 the ‘Tukey’ method. ***p < 0.001. Statistical tests included unpaired Student’s t test (A). Data in
485 (E, F, H, and I) were compared using the Mann-Whitney-U-test, and linear regressions in (G)
486 were compared using the F-test. n values are given in brackets.

487

488 **Figure 6. Lack of CaMK1D reduces ghrelin-induced AgRP/NPY expression and abundance**
489 **in AgRP neuron projections to the PVN.** (A) Representative Phos-tag immunoblot of CaMK1D

490 using lysates of hypothalamic cells from mice with indicated genotypes treated with 1 μ M Ghrelin
491 or vehicle for 5 min. Vinculin was used as a loading control. (B) Representative immunoblot of
492 pS179/T180 CaMK1D using lysates of whole hypothalamus from mice with indicated genotypes.
493 Animals were injected with 30 μ g ghrelin or vehicle and 2H after injections whole hypothalamus
494 was removed and used for protein extraction. GAPDH was used as a loading control. (C)
495 Representative immunoblots of pS79-ACC, pT172-AMPK and pS133-CREB using lysates of
496 hypothalamic primary neurons from mice with indicated genotypes treated with 1 μ M Ghrelin or
497 vehicle for 5 min. GAPDH was used as a loading control. (D) Expression of AgRP, NPY and
498 POMC mRNA in whole hypothalamus. Animals were injected with 30 μ g ghrelin or vehicle and
499 whole hypothalamus was removed 2H after injections. Tissues from mice with indicated genotypes
500 were analyzed by qPCR (n=5 to 6 / group). (E-F) Representative immunofluorescence and
501 quantification of AgRP projections to the PVN of mice with indicated genotypes. Animals were
502 injected with 30 μ g ghrelin and 2H after injections, whole hypothalamus was removed or brain was
503 extracted and sliced. (G) Schematic model depicting mechanisms as to how CaMK1D promotes
504 food intake.

505 *p < 0.05 and ***p < 0.001. Statistical tests included unpaired Student's t test (D,E).

506

507 **Supp Figure 1. Global deletion of *CaMK1D* in mice does not affect body size and *CaMK1D***
508 **knockout mice are born without any gross abnormalities.** (A) Knockout-first targeting strategy
509 within the *CaMK1D* locus and generation of floxed and total knockout mice. For further details
510 see material and methods. (B) Gender distribution of mice and (C) Mendelian ratios of born mice
511 with indicated genotypes. (D) Body length and (E) Tibia Length measurements of 7-week-old
512 mice with indicated genotypes (n=6 to 7 / group).

513

514 **Supp Figure 2. CaMK1D signaling is redundant in pancreatic beta cell and liver function.**

515 (A) Blood insulin levels during IPGTTs in mice with indicated genotypes on a HFD. IPGTT was
516 performed after an overnight food withdrawal. (n=11 to 11 / group). (B) Glucose-stimulated insulin
517 secretion (GSIS) in pancreatic islets isolated from mice with indicated genotypes. (n=6 to 7 /
518 group). (C) Expression of CaMK1D protein in pancreas and brain from mice with indicated
519 genotypes. Tissues were analyzed for CaMK1D expression by western blot. (D) Body weight gain
520 of mice with indicated genotypes on a Chow diet (CD) or on a High Fat Diet (HFD). (n=9 to 11/
521 group). (E-F) Blood glucose levels during IPGTTs in mice with indicated genotypes on a CD (E)
522 or on a HFD (F). IPGTT was performed after overnight food withdrawal. (n=9 to 11 / group).
523 (G) Expression of CaMK1D mRNA in liver from mice with indicated genotypes by qPCR. (H)
524 Body weight gain of mice with indicated genotypes on a CD or on a HFD. (n=9 to 11/ group).
525 Blood glucose levels during an IPGTT in mice with indicated genotypes on a CD (I) or on a HFD
526 (J). IPGTT was performed after overnight food withdrawal. (n=9 to 11 / group). Blood glucose
527 levels during an ITT in mice with indicated genotypes on a CD (K) or on a HFD (L). IPGTT was
528 performed 4H after food withdrawal. (n=6 to 10 / group).

529

530 **Supp Figure 3. Deletion of *CaMK1D* does not result in anxiety-like behavior and stress-**
531 **induced anhedonia.** (A) Distance traveled each 5 min, and (B) in total. (C) Rear number each 5
532 min, and (D) in total. (E) Number of entries in the center or periphery of the arena. (F) Time spent
533 in the center or periphery of the arena. (G) Average speed during an open field test. (n=9 / group).
534 (H) Amount of sucrose and water consumed over 3 day in while sucrose and water were both
535 available in the same time.

536

537 **Supp Figure 4. Deletion of *CaMK1D* in the Nervous Tissue reproduces phenotypes in whole-**
538 **body knockout mice.** (A) Expression of CaMK1D protein in different tissues in mice. Tissues
539 from mice with indicated genotypes were analyzed for CaMK1D expression by western blot. (B)

540 Body weight gain of mice with indicated genotypes on a Chow diet (CD) or on a High Fat Diet
541 (HFD). (n=10 to 15/ group). Cumulative food intake of mice with indicated genotypes on (C) CD
542 or on (D) HFD. (n=10 to 15 / group) (* $p \leq 0.05$). (E) Cumulative food intake of mice with indicated
543 genotypes and diets. Food intake was determined 24H after fasting. (n=12 to 17 / group). (F)
544 Cumulative food intake after ghrelin injection (30 μg / day) in mice with indicated genotypes on a
545 CD. (n=6 to 7 / group). * $p < 0.05$, ** $p < 0.01$ and *** $p < 0.001$. Statistical tests included two-way
546 ANOVA (B,C,D), and unpaired Student's t test (E,F).

547

548

549 **Supp Figure 5. Deletion of *CaMK1D* in POMC neurons does not affect energy metabolism in**
550 **mice.** (A) Verification of recombination in the *CaMK1D* locus in hypothalamus (Hyp), cortex
551 (Ctx), liver, tail and white blood cells (WBC) from mice with indicated genotypes. DNA from
552 tissues were analyzed by PCR with primers amplifying either recombined or floxed alleles,
553 respectively. (B) Body weight gain of mice with indicated genotypes on a Chow diet (CD) or on a
554 High Fat Diet (HFD). (n=10 to 15/ group).(C) Cumulative food intake of mice with indicated
555 genotypes on a CD. (n=10 to 15 / group). (D) Cumulative food intake of mice with indicated
556 genotypes on a HFD. (n=10 to 15 / group). (E) Cumulative food intake of mice with indicated
557 genotypes and diets. Food intake was determined 24H after fasting. (n=12 to 17 / group). (F)
558 Cumulative food intake after ghrelin injection in mice with indicated genotypes and diets. (n=6 to
559 7 / group). * $p < 0.05$. Statistical tests included unpaired Student's t test (F).

560

561 **Materials and Methods**

562 **Animals Care**

563 Animal care and all experimental procedures done in this study were approved by the local
564 ethical committee (Com'Eth) in compliance with the French and European legislation on care

565 and use of laboratory animals (APAFIS#18638-2019012510177514v4). Mice were
566 individually housed under controlled temperature at 22°C on a 12H light/dark cycle with
567 unrestricted access to water and prescribed diet. Food was only withdrawn if required for an
568 experiment. Body weight and food intake were determined weekly. Animals were fed with
569 regular chow diet (CD) or high fat diet (HFD). CD contains 73.6% calories from carbohydrates,
570 18.1% calories from protein, and 8.4% calories from fat (SAFE® D04 from Safe) and HFD
571 contains 20% calories from carbohydrates, 20% calories from protein, and 60% calories from
572 fat (D12492i from Research diet®). For all experiments only male mice were used. All
573 experiments were performed in adult mice at the age between 5-25 weeks.

574

575 **Generation of Transgenic Mice**

576 *CaMK1D* conditional knockout and global knockout mice were generated according to the
577 “knockout first” strategy by the Institut Clinique de la Souris (ICS, Illkirch-Graffenstaden,
578 France). 5’ of exon 4 of the *CaMK1D* gene a SA-βGeo-pA trapping cassette was inserted
579 flanked by two FRT sites, which disrupts gene function (“knockout first” allele and L3 mice).
580 Furthermore, two LoxP sites were inserted 5’ and 3’ of exon 4. The FRT-recombinase (Flp)
581 converted the “knockout first” allele to a conditional allele (*CaMK1D^{lox/lox}*), restoring gene
582 activity (Fig S1A). The sequences of the primers used to genotype the mice and to verify Cre-
583 mediated recombination are provided in Table S1. *CaMK1D^{lox/lox}* mice were mated with
584 Rosa26-Cre mice expressing Cre recombinase under control of the Rosa26 promoter (for global
585 knockout) (Soriano, 1999) resulting in the deletion of the floxed exon. The breeding colonies
586 were maintained by mating hemizygote *CaMK1D^{+/-}* females to hemizygote *CaMK1D^{+/-}* males.
587 Mice were on a C57BL/6 N/J mixed background. Tissue-specific deletion of *CaMK1D* was
588 obtained by mating floxed mice with transgenic mice expressing Cre recombinase under the
589 control of a tissue-specific promoter and breeding colonies were maintained by mating tissue-

590 specific promoter $Cre^{+};CaMKID^{flox/+}$ to $CaMKID^{flox/+}$ mice. All Mice were on a C57BL/6 N/J
591 mixed background. All cre deleter mouse lines are listed in the STAR methods section.

592

593 **Blood collection and biochemical measurements**

594 Blood samples obtained from the tail and collected in heparinized capillaries were used to
595 measure fasted blood glucose and insulin levels. Animals were fasted at 8 am, and the samples
596 were collected 4 hours later. At the end of the experiment, blood was collected from the retro
597 orbital sinus, put into tubes containing 0.2 μ M EDTA and 4 mM Pefabloc® SC, and centrifuged
598 for 15 minutes at 3,000 g to separate the plasma. Plasma was stored at -80°C . Acylated Ghrelin
599 Leptin and Insulin were measured by ELISA.

600

601 **Glucose and Insulin Tolerance Assays**

602 GTT: After a 16H fast, animals were injected i.p. with 2 g/kg (animals on CD) or 1 g/kg
603 (animals on HFD) dextrose in 0.9% NaCl. Blood glucose was measured prior to and 15, 30,
604 45, 60, 90, and 120 minutes after injections. Blood glucose values were determined in a drop
605 of blood sampled from the tail using an automatic glucose monitor (Accu-Check; Roche
606 Applied Science). Plasma samples were collected at 0, 15, 30 minutes for insulin
607 measurements.

608

609 ITT: After a 5-hour fast, animals were injected i.p. with 0.75 IU/kg recombinant human insulin
610 (Umluline; Lilly®). Blood glucose levels were measured before and 15, 30, 40, 60 and 90
611 minutes after injections. The glucose disappearance rate for the ITT (kITT)
612 (percentage/minute) was calculated using the formula as previously described (Lundbaek,
613 1962). $kITT = 0.693 \times 100 / t_{1/2}$, where $t_{1/2}$ was calculated from the slope of the plasma

614 glucose concentration, considering an exponential decrement of glucose concentration during
615 the 30 minutes after insulin administration.

616

617 **Automated Cages Phenotyping for indirect calorimetric measurements**

618 Twenty-five weeks old mice were acclimated in metabolic chambers (TSE LabMaster System
619 - Metabolic Phenotyping Facility, ICS) for 1 day before the start of the recordings. Mice were
620 continuously recorded for 1 or 2 days with measurements of locomotor activity (in the xy- and
621 z-axes), and gas exchange (O₂ and CO₂) every 30 min. Energy expenditure was calculated
622 according to the manufacturer's guidelines (PhenoMaster Software, TSE System). The
623 respiratory quotient was estimated by calculating the ratio of CO₂ production to O₂
624 consumption. Values were corrected by metabolic mass (lean mass + 0.2 fat mass) as
625 previously described (Even and Nadkarni, 2012). ANCOVA analysis was done as previously
626 described (Müller et al., 2021).

627

628 **Animal length and body composition**

629 Animal length was assessed with X-Ray MX-20 Specimen (Faxitron - Metabolic Phenotyping
630 Facility, ICS). Digital X-ray pictures allowed the measurement of whole body and tibia size of
631 mice. Body composition was evaluated by Quantitative Nuclear Magnetic Resonance (qNMR)
632 using Minispec⁺ analyzer (Bruker BioSpin S.A.S., Metabolic Phenotyping Facility, ICS).

633

634 **Leptin/ghrelin responsiveness**

635 To assess leptin sensitivity, mice received an i.p. injection of either PBS or mouse recombinant
636 leptin (3 mg/kg) 24H after food withdrawal, their food intake were monitored 4 and 6H
637 following the injections. The food intake after PBS injection was compared with the food intake
638 after leptin administration. The orexigenic response to ghrelin was determined in mice that

639 received an i.p injection of either PBS or ghrelin (1 mg/kg). Food intake was assessed 4H and
640 6H after injections.

641

642 **Culture of primary cells of hypothalamus**

643 Hypothalamus were dissected from E15.5 embryos and stored on ice in Neurobasal medium
644 (GIBCO). Tissues were incubated for 20 min in a 37°C water bath in 100U/ml papain
645 (Worthington) and 10mg/ml DNase I (Worthington). Digestion was stopped with
646 Ovomucoide (Worthington). Tissues were transferred into 1 ml of adult neuronal growth
647 medium consisting of Neurobasal-A medium, 3mM L-glutamine (Gibco) , 1x B-27
648 supplement, 1x N2 supplement and antibiotics. Tissues were gently triturated until uniform
649 cellular dissociation was achieved. Cells were counted and plated into cell culture plates coated
650 with poly-L-lysine (Gibco).

651

652 **Western blotting**

653 Cells were washed with ice-cold PBS on ice and snap-frozen in liquid nitrogen. Cell lysates for
654 WB were prepared using 1x Laemmli buffer (50 mM Tris-HCl pH6.8, 100 mM DTT, 8% SDS,
655 0,01% bromophenol blue, 10% glycerol) supplemented with phosphatase/protease inhibitors
656 (Cell Signaling Technology) and incubated on ice for 10 minutes. After centrifugation at 16
657 000 g for 10 minutes at 4°C cleared supernatant was transferred to the new tubes and was used
658 immediately stored at -80°C until used. Total protein was measured using the BCA method by
659 Pierce™ BCA Protein Assay Kit (ThermoFisher). Samples (20-50 µg of total protein content)
660 were boiled and resolved on 10% acrylamide gels using standard Tris-Glycine SDS-PAGE or
661 Phostag gels. Proteins were transferred to PVDF membranes (Millipore) and blotted with
662 antibodies listed in the Antibodies section. For membrane blocking and primary antibody
663 dilution 5% BSA (w/v) in TBST was used. All incubations with primary antibodies were

664 performed for 16 hours at 4°C. Blots were developed using SuperSignal West Pico (Pierce,
665 Ref. 34580) or Luminata Forte Western HRP substrate (Merck Millipore, Ref. WBLUF0500).

666

667 **Hypothalamic mRNA quantification**

668 Total RNA from hypothalamus was extracted using an RNeasy Lipid Tissue Mini Kit
669 (QIAGEN) and quantified spectrophotometrically. Single-stranded cDNA was synthesized
670 using SuperScript IV RNase Reverse Transcriptase (Invitrogen) according to the
671 manufacturer's directions. Real-time PCR was carried out using an LightCycler® 480 (Roche)
672 with Fast SYBR® Green Master Mix (Roche) and the primers listed in the primers section.
673 Quantifications were done according the Pfaffl method (Pfaffl, 2001).

674

675 **Immunohistochemistry**

676 Mediobasal hypothalamic sections from brains were prefixed with paraformaldehyde during
677 24h and incubated in 30% sucrose (Fisher Scientific) 24H at 4°C. Brains were embedded in
678 OCT, frozen at -80°C and stored at -80°C. 30 µm-thick sections were cut with a cryostat (Leica
679 CM3050 S, France), stored at 4°C in sodium phosphate buffer. Sections were processed as
680 follows: Day 1: free-floating sections were rinsed in PBS, incubated for 20 min in PBS
681 containing 0.3% Tween-20, and then rinsed three times for 10 min each in PBS. Slices were
682 incubated 1h with 5% donkey serum in 0.3% PBS-T and then overnight or 72H at 4°C with the
683 primary antibodies described in the antibodies section. Slides were rinsed three times for 10
684 min in 0.3% PBS-T and incubated for 60 min with secondary antibodies. Sections were rinsed
685 three times for 10 min in PBS before mounting. Tissues were observed on a confocal laser
686 scanning microscope , TCS SP8X; with Leica software LAS X navigator, using a HC PL APO
687 CS2 20x /0.75 dry leica objective. The objectives and the pinhole setting (1 airy unit, au)
688 remained unchanged during the acquisition of a series for all images. Quantification of

689 immuno-positive cells was performed using the cell counter plugin of the ImageJ software
690 taking as standard reference a fixed threshold of fluorescence.

691

692 **Electrophysiology**

693 Experiments were performed on brain slices from 9-12 week old male CaMK1D^{+/+} and
694 CaMK1D^{-/-} mice that expressed enhanced green fluorescent protein (EGFP) selectively in
695 AgRP neurons. Animals were kept under standard laboratory conditions, with tap water and
696 chow available ad libitum, on a 12h light/dark cycle. The animals were lightly anesthetized
697 with isoflurane (B506; AbbVie Deutschland GmbH and Co KG, Ludwigshafen, Germany) and
698 decapitated. Coronal slices (280 μ m) containing the arcuate nucleus of the hypothalamus were
699 cut with a vibration microtome (VT1200 S; Leica, Germany) under cold (4°C), carbogenated
700 (95% O₂ and 5% CO₂), glycerol-based modified artificial cerebrospinal fluid (GaCSF) (Ye et
701 al., 2006).

702 Current-clamp recordings of GFP-expressing AgRP neurons were performed at ~32°C.
703 Neurons were visualized with a fixed stage upright microscope (Zeiss AxioExaminer, Zeiss,
704 Germany) using 40x water-immersion objective (W Plan-Apochromat 40x/1.0 DIC M27, 1
705 numerical aperture, 2.5 mm working distance; Zeiss) with infrared differential interference
706 contrast optics (Dodt and Zieglgänsberger, 1990) and fluorescence optics. GFP-expressing
707 AgRP neurons were identified by their anatomical location in the arcuate nucleus and by their
708 fluorescent label.

709 Perforated patch experiments were conducted using protocols modified from (Horn and Marty,
710 1988) and (Akaike and Harata, 1994).

711 The spontaneous firing frequency was measured for 5 min after perforation. To measure
712 intrinsic electrophysiological properties series of hyperpolarizing and depolarizing current
713 pulses were applied under current clamp from a membrane potential of ~-70 mV. For input

714 resistance and capacitance measurements, hyperpolarizing current steps with -2 pA increments
715 were applied. For excitability measurements, depolarizing 1 s current steps with +2 pA
716 increments were applied. The specific protocols are given in Results.

717 To investigate the modulatory effect of ghrelin (031-31, Phoenix Pharmaceuticals), 100 nM
718 ghrelin was bath applied for 8-10 min. The ghrelin effect was analyzed by comparing the action
719 potential frequencies that were measured during 2 min intervals that were recorded directly
720 before and at the end of the peptide applications.

721 **Data analysis of electrophysiological data**

722 Data analysis was performed with Spike2 (version 7; Cambridge Electronic Design Ltd.,
723 Cambridge, UK), Igor Pro 6 (Wavemetrics, Portland, OR, USA), and Graphpad Prism 8. If not
724 stated otherwise, all calculated values are expressed as means \pm SEM (standard error of the
725 mean). The horizontal lines show the data's median. The whiskers were calculated according
726 to the 'Tukey' method. For comparisons of independent nonparametric distributions, the
727 Mann-Whitney-U-test was used. Linear regressions were compared using the F-test. A
728 significance level of 0.05 was accepted for all tests. Exact p-values are reported if $p > 0.05$. In
729 the figures, n values are given in brackets.

730

731 **Quantification and statistical analysis**

732 All statistical comparisons were performed with Prism 6 (GraphPad Software, La Jolla, CA,
733 USA) or R software for ANCOVA analysis. The statistical tests used are listed along with the
734 statistical values in the Supplemental Tables. All the data were analyzed using either Student t
735 test (paired or unpaired) with equal variances or One-way ANOVA or Two-way ANOVA. In
736 all cases, significance threshold was automatically set at $p < 0.05$. ANOVA analyses were
737 followed by Bonferroni post hoc test for specific comparisons only when overall ANOVA
738 revealed a significant difference (at least $p < 0.05$).

739

740 **STAR METHODS**

Antibodies

Rabbit polyclonal anti-CaMK1D	This study	N/A
Rabbit polyclonal anti-phospho-Ser179/T180 CaMK1D	This study	N/A
Rabbit polyclonal anti-Phospho-Acetyl-CoA Carboxylase (Ser79)	Cell Signaling Technology	Cat# 3661, RRID:AB_330337
Rabbit polyclonal anti-Acetyl-CoA Carboxylase	Cell Signaling Technology	Cat# 3662, RRID:AB_2219400
Rabbit monoclonal anti-phospho-Thr172 AMPK	Cell Signaling Technology	Cat# 2535, RRID:AB_331250
Rabbit polyclonal anti-AMPK	Cell Signaling Technology	Cat# 2532, RRID:AB_330331
Rabbit monoclonal anti-phospho-Ser133 CREB	Cell Signaling Technology	Cat# 9198, RRID:AB_2561044
Rabbit monoclonal anti-CREB	Cell Signaling Technology	Cat# 9197, RRID:AB_331277
Rabbit monoclonal anti-cFOS	Cell signaling Technolgy	Cat# 2250, RRID:AB_2247211
Goat polyclonal anti Mouse AgRP/ART	R&D Systems	Cat# AF634, RRID:AB_2273824
Rabbit monoclonal anti-Vinculin	Cell Signaling Technology	Cat# 13901, RRID:AB_2728768
Rabbit polyclonal anti-GAPDH	Sigma-Aldrich	Cat# G9545, RRID:AB_796208
Peroxidase-AffiniPure Goat Anti-Rabbit IgG (H+L)	Jackson ImmunoResearch Labs	Cat# 111-035-144, RRID:AB_2307391
Goat anti-Rabbit IgG, Alexa Fluor 488	ThermoFisher Scientific	Cat# A-11037, RRID:AB_2534095
Donkey anti-Rabbit IgG, Alexa Fluor 488	Molecular Probes	Cat# A-21206, RRID:AB_2535792
Donkey anti-Goat IgG , Alexa Fluor 568	Molecular Probes	Cat# A-11057, RRID:AB_142581

Chemicals, Peptides, and Recombinant Proteins

Ghrelin (rat)	R&D Systems	Cat# 1465/1
Recombinant Mouse Leptin Protein	R&D Systems	Cat# 498-OB-05M
L-glutamine	Gibco™	Cat# 25030123
B-27 supplement	Gibco™	Cat# 17504044
N2 supplement	Gibco™	Cat# A1370701
Pencillin / Streptomycin	Gibco™	Cat# 15140130
Pefabloc® SC	Roche	Cat# 11429868001
Glucose	Euromedex	UG3050
Umulin	Lilly	HI0219
Papain	Worthington	WOLK03178
DNase I	Worthington	WOLK03172
poly-L-lysine	Gibco™	
phosphatase/protease inhibitors	Cell Signaling Technology	5872
Phostag gels	Sobioda	W1W195-17991
SuperSignal™ West Pico PLUS Chemiluminescent Substrate	ThermoFisher Scientific	34580

Luminata Forte Western HRP Substrate	MerckMillipore	WBLUF0500
SuperScript IV Reverse Transcriptase	Invitrogen	18090200
FastStart Essential DNA Green Master	Roche Life Science	06924204001
Critical Commercial Assays		
Mouse Ultrasensitive Insulin ELISA	Alpco®	80-INSMSU-E01
Rat/Mouse Ghrelin (active) ELISA	MerckMillipore	EZRGRA-90K
Leptin : MILLIPLEX MAP Rat Metabolic Hormone Magnetic Bead Panel - Metabolism Multiplex Assay	MerckMillipore	RMHMAG-84K-02
Pierce™ BCA Protein Assay Kit	ThermoFisher Scientific	23225
RNeasy® Lipid Tissue Mini Kit	Qiagen	74804
Experimental Models: Mouse Lines		
<i>CaMK1D^{flox/flox}</i>	This study	N/A
<i>B6.Cg-Tg(Nes-cre)1Kln/J = Nestin^{Cre/+}</i>	The Jackson Laboratory	Stock No: 003771
<i>Agrp^{tm1(cre)Lowl/J = AgRP^{Cre/+}}</i>	The Jackson Laboratory	Stock No: 012899
<i>B6.FVB-Tg(Pomc-cre)1Lowl/J = POMC^{Cre/+}</i>	The Jackson Laboratory	Stock No: 010714
<i>Tg(Pdx1-cre/Esr1*)#Dam/J = PDX1^{Cre/+}</i>	The Jackson Laboratory	Stock No: 024968
<i>B6.Cg-Speer6-ps1^{Tg(Alb-cre)21Mgn/J = Alb^{Cre/+}}</i>	The Jackson Laboratory	Stock No: 003574
<i>B6.FVB-Tg(Npy-hrGFP)1Lowl/J = NPY^{GFP}</i>	The Jackson Laboratory	Stock No: 006417
<i>Gt(ROSA)26Sor^{tm1(ACTB-cre,-EGFP)Ics = ROSA^{Cre/+}}</i>	ICS	MGI:3716464
Software and Algorithms		
Fiji Image Analysis	ImageJ	https://imagej.net/Fiji
Prism version 8.1.1	GraphPad	N/A
Primers (Genotyping)		
Forward CaMK1D Flox Allele	GTCTGAACATCTAAAGGGCACTCCTG	Wild Type Allele : 1122 bp Knock-out Allele : :277 bp
Reverse CaMK1D Flox Allele	ACTGATGGCGAGCTCAGACCATAAC	
Reverse CaMK1D Flox Allele	CCTACAGGCAATCCTTTAGAGGC	Wild Type Allele : 1147 bp Knock-out Allele : :452 bp
Forward Cre Transgene	CCATCTGCCACCAGCCAG	281 bp
Reverse Cre Transgene	TCGCCATCTTCCAGCAGG	
Primers (qPCR)		
Forward mAgRP	GCTCCACTGAAGGGCATCAGAA	

Reverse mAgRP	GGATCTAGCACCTCCGCCAAA
Forward mNPY	CCGCTCTGCGACACTACAT
Reverse mNPY	TGTCTCAGGGCTGGATCTCT
Forward mPOMC	CCCGCCCAAGGACAAGCGTT
Reverse mPOMC	CTGGCCCTTCTTGTGCGCGT
Forward mCaMK1D	CTCGACACCCATGGATTGCT
Reverse mCaMK1D	ACTACAGAGCGTGGAAGGTG
Forward mTBP	TGCTGTTGGTGATTGTTGGT
Reverse-mTBP	CTGGCTTGTGTGGGAAAGAT

741

742 **Acknowledgments**

743 We thank T. Alquier at University of Montreal, E. Pangou and D. Dembele at the IGBMC for
744 helpful discussions. We thank the Imaging Center of the IGBMC (ICI) and the IGBMC core
745 facilities for their support on this research. We are grateful to F. Berditchevski at Nottingham
746 University for the pS179/Thr180 CaMK1D antibody. This work was supported by the Agence
747 Nationale de la Recherche (ANR) (AAPG 2017 LYSODIABETES and AAPG 2021
748 HypoCaMK)), by the Fondation de Recherche Médicale (FRM) – Program: Equipe FRM
749 (EQU201903007859, Prix Roger PROPICE pour la recherche sur le cancer du pancréas), by
750 the FHU-OMAGE of region Grand-Est, from the European Foundation for the Study of
751 Diabetes (EFSD)/Novo Nordisk Diabetes Research Programme and by the ANR-10-LABX-
752 0030-INRT grant as well as the ANR-11-INBS-0009-INGESTEM grant, both French State
753 funds managed by the ANR under the frame program Investissements d’Avenir. K. Vivot was
754 supported by an Individual Fellowship (798961 INSULYSOSOME) in the framework of the
755 Marie-Sklodovska Curie actions of the European Commission. G. Yeghiazaryan received
756 financial doctoral support from DFG-233886668/RTG1960.

757

758

759 **Author contributions**

760 Conceptualization: R.R., R.P.N, P.K and S.L., Software: E.G., Methodology: K.V., Z.Z, G.Y.,
761 E.E., E.C.C. and M.Q, Validation: K.V., Formal Analysis: K.V., C.M., Investigation: K.V.,
762 G.M., Z.Z., E.E., G.Y., M.Q., A.S., M.F and C.M., Resources: E.E., Writing-Original Draft:
763 R.R. and K.V., Supervision: S.L., P.K., R.P.R., A.C., and R.R, Funding Acquisition: R.R. and
764 S.L.

765

766 **References**

767 Akaike, N., and Harata, N. (1994). Nystatin perforated patch recording and its applications to
768 analyses of intracellular mechanisms. *Jpn J Physiol* *44*, 433–473.

769 Albert, V., Cornu, M., and Hall, M.N. (2015). mTORC1 signaling in *Agrp* neurons mediates
770 circadian expression of *Agrp* and NPY but is dispensable for regulation of feeding behavior.
771 *Biochem Biophys Res Commun* *464*, 480–486.

772 Anderson, K.A., Ribar, T.J., Lin, F., Noeldner, P.K., Green, M.F., Muehlbauer, M.J., Witters,
773 L.A., Kemp, B.E., and Means, A.R. (2008). Hypothalamic CaMKK2 contributes to the
774 regulation of energy balance. *Cell Metab.* *7*, 377–388.

775 Andersson, U., Filipsson, K., Abbott, C.R., Woods, A., Smith, K., Bloom, S.R., Carling, D.,
776 and Small, C.J. (2004). AMP-activated protein kinase plays a role in the control of food
777 intake. *J Biol Chem* *279*, 12005–12008.

778 Andrews, Z.B., Liu, Z.-W., Wallingford, N., Erion, D.M., Borok, E., Friedman, J.M.,
779 Tschöp, M.H., Shanabrough, M., Cline, G., Shulman, G.I., et al. (2008). UCP2 mediates
780 ghrelin's action on NPY/AgRP neurons by lowering free radicals. *Nature* *454*, 846–851.

781 Aponte, Y., Atasoy, D., and Sternson, S.M. (2011). AGRP neurons are sufficient to
782 orchestrate feeding behavior rapidly and without training. *Nat Neurosci* *14*, 351–355.

783 Bonnefond, A., and Froguel, P. (2015). Rare and common genetic events in type 2 diabetes:
784 what should biologists know? *Cell Metab.* *21*, 357–368.

785 Bouret, S.G., Draper, S.J., and Simerly, R.B. (2004). Formation of projection pathways from
786 the arcuate nucleus of the hypothalamus to hypothalamic regions implicated in the neural
787 control of feeding behavior in mice. *J Neurosci* *24*, 2797–2805.

788 Buchser, W.J., Slepak, T.I., Gutierrez-Arenas, O., Bixby, J.L., and Lemmon, V.P. (2010).
789 Kinase/phosphatase overexpression reveals pathways regulating hippocampal neuron
790 morphology. *Mol. Syst. Biol.* *6*, 391.

791 Chen, H.Y., Trumbauer, M.E., Chen, A.S., Weingarth, D.T., Adams, J.R., Frazier, E.G.,
792 Shen, Z., Marsh, D.J., Feighner, S.D., Guan, X.-M., et al. (2004). Orexigenic action of

- 793 peripheral ghrelin is mediated by neuropeptide Y and agouti-related protein. *Endocrinology*
794 *145*, 2607–2612.
- 795 Chen, S.-R., Chen, H., Zhou, J.-J., Pradhan, G., Sun, Y., Pan, H.-L., and Li, D.-P. (2017).
796 Ghrelin receptors mediate ghrelin-induced excitation of agouti-related protein/neuropeptide Y
797 but not pro-opiomelanocortin neurons. *J. Neurochem.* *142*, 512–520.
- 798 Denis, R.G.P., Joly-Amado, A., Cansell, C., Castel, J., Martinez, S., Delbes, A.S., and
799 Luquet, S. (2014). Central orchestration of peripheral nutrient partitioning and substrate
800 utilization: implications for the metabolic syndrome. *Diabetes Metab* *40*, 191–197.
- 801 Dodt, H.U., and Zieglgänsberger, W. (1990). Visualizing unstained neurons in living brain
802 slices by infrared DIC-videomicroscopy. *Brain Res* *537*, 333–336.
- 803 Even, P.C., and Nadkarni, N.A. (2012). Indirect calorimetry in laboratory mice and rats:
804 principles, practical considerations, interpretation and perspectives. *Am J Physiol Regul*
805 *Integr Comp Physiol* *303*, R459-476.
- 806 Flavell, S.W., and Greenberg, M.E. (2008). Signaling mechanisms linking neuronal activity
807 to gene expression and plasticity of the nervous system. *Annu Rev Neurosci* *31*, 563–590.
- 808 García, A., Alvarez, C.V., Smith, R.G., and Diéguez, C. (2001). Regulation of Pit-1
809 expression by ghrelin and GHRP-6 through the GH secretagogue receptor. *Mol Endocrinol*
810 *15*, 1484–1495.
- 811 Gonzalez, G.A., and Montminy, M.R. (1989). Cyclic AMP stimulates somatostatin gene
812 transcription by phosphorylation of CREB at serine 133. *Cell* *59*, 675–680.
- 813 Gu, G., Dubauskaite, J., and Melton, D.A. (2002). Direct evidence for the pancreatic lineage:
814 NGN3+ cells are islet progenitors and are distinct from duct progenitors. *Development* *129*,
815 2447–2457.
- 816 Haney, S., Zhao, J., Tiwari, S., Eng, K., Guey, L.T., and Tien, E. (2013). RNAi screening in
817 primary human hepatocytes of genes implicated in genome-wide association studies for roles
818 in type 2 diabetes identifies roles for CAMK1D and CDKAL1, among others, in hepatic
819 glucose regulation. *PLoS ONE* *8*, e64946.
- 820 Haribabu, B., Hook, S.S., Selbert, M.A., Goldstein, E.G., Tomhave, E.D., Edelman, A.M.,
821 Snyderman, R., and Means, A.R. (1995). Human calcium-calmodulin dependent protein
822 kinase I: cDNA cloning, domain structure and activation by phosphorylation at threonine-177
823 by calcium-calmodulin dependent protein kinase I kinase. *EMBO J* *14*, 3679–3686.
- 824 Hoffman, G.E., Smith, M.S., and Verbalis, J.G. (1993). c-Fos and related immediate early
825 gene products as markers of activity in neuroendocrine systems. *Front Neuroendocrinol* *14*,
826 173–213.
- 827 Horn, R., and Marty, A. (1988). Muscarinic activation of ionic currents measured by a new
828 whole-cell recording method. *J Gen Physiol* *92*, 145–159.
- 829 Jais, A., and Brüning, J.C. (2021). Arcuate nucleus-dependent regulation of metabolism -
830 pathways to obesity and diabetes mellitus. *Endocr Rev* bna025.

- 831 Kamata, A., Sakagami, H., Tokumitsu, H., Owada, Y., Fukunaga, K., and Kondo, H. (2007).
832 Spatiotemporal expression of four isoforms of Ca²⁺/calmodulin-dependent protein kinase I
833 in brain and its possible roles in hippocampal dendritic growth. *Neurosci. Res.* *57*, 86–97.
- 834 Kim, K.-S., Seeley, R.J., and Sandoval, D.A. (2018). Signalling from the periphery to the
835 brain that regulates energy homeostasis. *Nat. Rev. Neurosci.* *19*, 185–196.
- 836 Kohno, D., Gao, H.-Z., Muroya, S., Kikuyama, S., and Yada, T. (2003). Ghrelin directly
837 interacts with neuropeptide-Y-containing neurons in the rat arcuate nucleus: Ca²⁺ signaling
838 via protein kinase A and N-type channel-dependent mechanisms and cross-talk with leptin
839 and orexin. *Diabetes* *52*, 948–956.
- 840 Kola, B., Hubina, E., Tucci, S.A., Kirkham, T.C., Garcia, E.A., Mitchell, S.E., Williams,
841 L.M., Hawley, S.A., Hardie, D.G., Grossman, A.B., et al. (2005). Cannabinoids and ghrelin
842 have both central and peripheral metabolic and cardiac effects via AMP-activated protein
843 kinase. *J Biol Chem* *280*, 25196–25201.
- 844 Könnner, A.C., Janoschek, R., Plum, L., Jordan, S.D., Rother, E., Ma, X., Xu, C., Enriori, P.,
845 Hampel, B., Barsh, G.S., et al. (2007). Insulin action in AgRP-expressing neurons is required
846 for suppression of hepatic glucose production. *Cell Metab* *5*, 438–449.
- 847 Kooner, J.S., Saleheen, D., Sim, X., Sehmi, J., Zhang, W., Frossard, P., Been, L.F., Chia, K.-
848 S., Dimas, A.S., Hassanali, N., et al. (2011). Genome-wide association study in individuals of
849 South Asian ancestry identifies six new type 2 diabetes susceptibility loci. *Nat. Genet.* *43*,
850 984–989.
- 851 Locke, A.E., Kahali, B., Berndt, S.I., Justice, A.E., Pers, T.H., Day, F.R., Powell, C.,
852 Vedantam, S., Buchkovich, M.L., Yang, J., et al. (2015). Genetic studies of body mass index
853 yield new insights for obesity biology. *Nature* *518*, 197–206.
- 854 López, M., Lage, R., Saha, A.K., Pérez-Tilve, D., Vázquez, M.J., Varela, L., Sangiao-
855 Alvarellós, S., Tovar, S., Raghay, K., Rodríguez-Cuenca, S., et al. (2008). Hypothalamic fatty
856 acid metabolism mediates the orexigenic action of ghrelin. *Cell Metab* *7*, 389–399.
- 857 Lundbaek, K. (1962). Intravenous glucose tolerance as a tool in definition and diagnosis of
858 diabetes mellitus. *Br Med J* *1*, 1507–1513.
- 859 Luquet, S., Perez, F.A., Hnasko, T.S., and Palmiter, R.D. (2005). NPY/AgRP neurons are
860 essential for feeding in adult mice but can be ablated in neonates. *Science* *310*, 683–685.
- 861 Martins, L., Fernández-Mallo, D., Novelle, M.G., Vázquez, M.J., Tena-Sempere, M.,
862 Nogueiras, R., López, M., and Diéguez, C. (2012). Hypothalamic mTOR signaling mediates
863 the orexigenic action of ghrelin. *PLoS One* *7*, e46923.
- 864 Morris, A.P., Voight, B.F., Teslovich, T.M., Ferreira, T., Segrè, A.V., Steinthorsdottir, V.,
865 Strawbridge, R.J., Khan, H., Gallert, H., Mahajan, A., et al. (2012). Large-scale association
866 analysis provides insights into the genetic architecture and pathophysiology of type 2
867 diabetes. *Nat. Genet.* *44*, 981–990.
- 868 Morton, G.J., Cummings, D.E., Baskin, D.G., Barsh, G.S., and Schwartz, M.W. (2006).
869 Central nervous system control of food intake and body weight. *Nature* *443*, 289–295.

- 870 Müller, T.D., Nogueiras, R., Andermann, M.L., Andrews, Z.B., Anker, S.D., Argente, J.,
871 Batterham, R.L., Benoit, S.C., Bowers, C.Y., Broglio, F., et al. (2015). Ghrelin. *Mol Metab* 4,
872 437–460.
- 873 Müller, T.D., Klingenspor, M., and Tschöp, M.H. (2021). Revisiting energy expenditure: how
874 to correct mouse metabolic rate for body mass. *Nat Metab* 3, 1134–1136.
- 875 Nakazato, M., Murakami, N., Date, Y., Kojima, M., Matsuo, H., Kangawa, K., and
876 Matsukura, S. (2001). A role for ghrelin in the central regulation of feeding. *Nature* 409, 194–
877 198.
- 878 Pfaffl, M.W. (2001). A new mathematical model for relative quantification in real-time RT-
879 PCR. *Nucleic Acids Res* 29, e45.
- 880 Postic, C., Shiota, M., Niswender, K.D., Jetton, T.L., Chen, Y., Moates, J.M., Shelton, K.D.,
881 Lindner, J., Cherrington, A.D., and Magnuson, M.A. (1999). Dual roles for glucokinase in
882 glucose homeostasis as determined by liver and pancreatic beta cell-specific gene knock-outs
883 using Cre recombinase. *J Biol Chem* 274, 305–315.
- 884 Sakkou, M., Wiedmer, P., Anlag, K., Hamm, A., Seuntjens, E., Ettwiller, L., Tschöp, M.H.,
885 and Treier, M. (2007). A role for brain-specific homeobox factor Bsx in the control of
886 hyperphagia and locomotory behavior. *Cell Metab* 5, 450–463.
- 887 Schmitt, J.M., Guire, E.S., Saneyoshi, T., and Soderling, T.R. (2005). Calmodulin-dependent
888 kinase kinase/calmodulin kinase I activity gates extracellular-regulated kinase-dependent
889 long-term potentiation. *J. Neurosci.* 25, 1281–1290.
- 890 Senga, Y., Ishida, A., Shigeri, Y., Kameshita, I., and Sueyoshi, N. (2015). The Phosphatase-
891 Resistant Isoform of CaMKI, Ca²⁺/Calmodulin-Dependent Protein Kinase Iδ (CaMKIδ),
892 Remains in Its “Primed” Form without Ca²⁺ Stimulation. *Biochemistry* 54, 3617–3630.
- 893 Sheng, M., Thompson, M.A., and Greenberg, M.E. (1991). CREB: a Ca(2+)-regulated
894 transcription factor phosphorylated by calmodulin-dependent kinases. *Science* 252, 1427–
895 1430.
- 896 Shu, X.O., Long, J., Cai, Q., Qi, L., Xiang, Y.-B., Cho, Y.S., Tai, E.S., Li, X., Lin, X., Chow,
897 W.-H., et al. (2010). Identification of new genetic risk variants for type 2 diabetes. *PLoS*
898 *Genet.* 6, e1001127.
- 899 Simonis-Bik, A.M., Nijpels, G., van Haeften, T.W., Houwing-Duistermaat, J.J., Boomsma,
900 D.I., Reiling, E., van Hove, E.C., Diamant, M., Kramer, M.H.H., Heine, R.J., et al. (2010).
901 Gene variants in the novel type 2 diabetes loci CDC123/CAMK1D, THADA, ADAMTS9,
902 BCL11A, and MTNR1B affect different aspects of pancreatic beta-cell function. *Diabetes* 59,
903 293–301.
- 904 Soriano, P. (1999). Generalized lacZ expression with the ROSA26 Cre reporter strain. *Nat*
905 *Genet* 21, 70–71.
- 906 Steculorum, S.M., Collden, G., Coupe, B., Croizier, S., Lockie, S., Andrews, Z.B., Jarosch,
907 F., Klussmann, S., and Bouret, S.G. (2015). Neonatal ghrelin programs development of
908 hypothalamic feeding circuits. *J Clin Invest* 125, 846–858.

- 909 Stevanovic, D., Trajkovic, V., Müller-Lüthloff, S., Brandt, E., Abplanalp, W., Bumke-Vogt,
910 C., Liehl, B., Wiedmer, P., Janjetovic, K., Starcevic, V., et al. (2013). Ghrelin-induced food
911 intake and adiposity depend on central mTORC1/S6K1 signaling. *Mol Cell Endocrinol* *381*,
912 280–290.
- 913 Stuber, G.D., and Wise, R.A. (2016). Lateral hypothalamic circuits for feeding and reward.
914 *Nat Neurosci* *19*, 198–205.
- 915 Takemoto-Kimura, S., Ageta-Ishihara, N., Nonaka, M., Adachi-Morishima, A., Mano, T.,
916 Okamura, M., Fujii, H., Fuse, T., Hoshino, M., Suzuki, S., et al. (2007). Regulation of
917 dendritogenesis via a lipid-raft-associated Ca²⁺/calmodulin-dependent protein kinase
918 CLICK-III/CaMKI γ . *Neuron* *54*, 755–770.
- 919 Thurner, M., van de Bunt, M., Torres, J.M., Mahajan, A., Nylander, V., Bennett, A.J.,
920 Gaulton, K.J., Barrett, A., Burrows, C., Bell, C.G., et al. (2018). Integration of human
921 pancreatic islet genomic data refines regulatory mechanisms at Type 2 Diabetes susceptibility
922 loci. *Elife* *7*.
- 923 Timper, K., and Brüning, J.C. (2017). Hypothalamic circuits regulating appetite and energy
924 homeostasis: pathways to obesity. *Dis Model Mech* *10*, 679–689.
- 925 Verploegen, S., Ulfman, L., van Deutekom, H.W.M., van Aalst, C., Honing, H., Lammers, J.-
926 W.J., Koenderman, L., and Coffey, P.J. (2005). Characterization of the role of CaMKI-like
927 kinase (CKLiK) in human granulocyte function. *Blood* *106*, 1076–1083.
- 928 Waterson, M.J., and Horvath, T.L. (2015). Neuronal Regulation of Energy Homeostasis:
929 Beyond the Hypothalamus and Feeding. *Cell Metab.* *22*, 962–970.
- 930 Wayman, G.A., Kaech, S., Grant, W.F., Davare, M., Impey, S., Tokumitsu, H., Nozaki, N.,
931 Banker, G., and Soderling, T.R. (2004). Regulation of axonal extension and growth cone
932 motility by calmodulin-dependent protein kinase I. *J. Neurosci.* *24*, 3786–3794.
- 933 Xue, A., Wu, Y., Zhu, Z., Zhang, F., Kemper, K.E., Zheng, Z., Yengo, L., Lloyd-Jones, L.R.,
934 Sidorenko, J., Wu, Y., et al. (2018). Genome-wide association analyses identify 143 risk
935 variants and putative regulatory mechanisms for type 2 diabetes. *Nat Commun* *9*, 2941.
- 936 Ye, J.H., Zhang, J., Xiao, C., and Kong, J.-Q. (2006). Patch-clamp studies in the CNS
937 illustrate a simple new method for obtaining viable neurons in rat brain slices: glycerol
938 replacement of NaCl protects CNS neurons. *J Neurosci Methods* *158*, 251–259.
- 939 Zeggini, E., Scott, L.J., Saxena, R., Voight, B.F., Marchini, J.L., Hu, T., de Bakker, P.I.,
940 Abecasis, G.R., Almgren, P., Andersen, G., et al. (2008). Meta-analysis of genome-wide
941 association data and large-scale replication identifies additional susceptibility loci for type 2
942 diabetes. *Nature Genetics* *40*, 638–645.
- 943
- 944

Figure 1

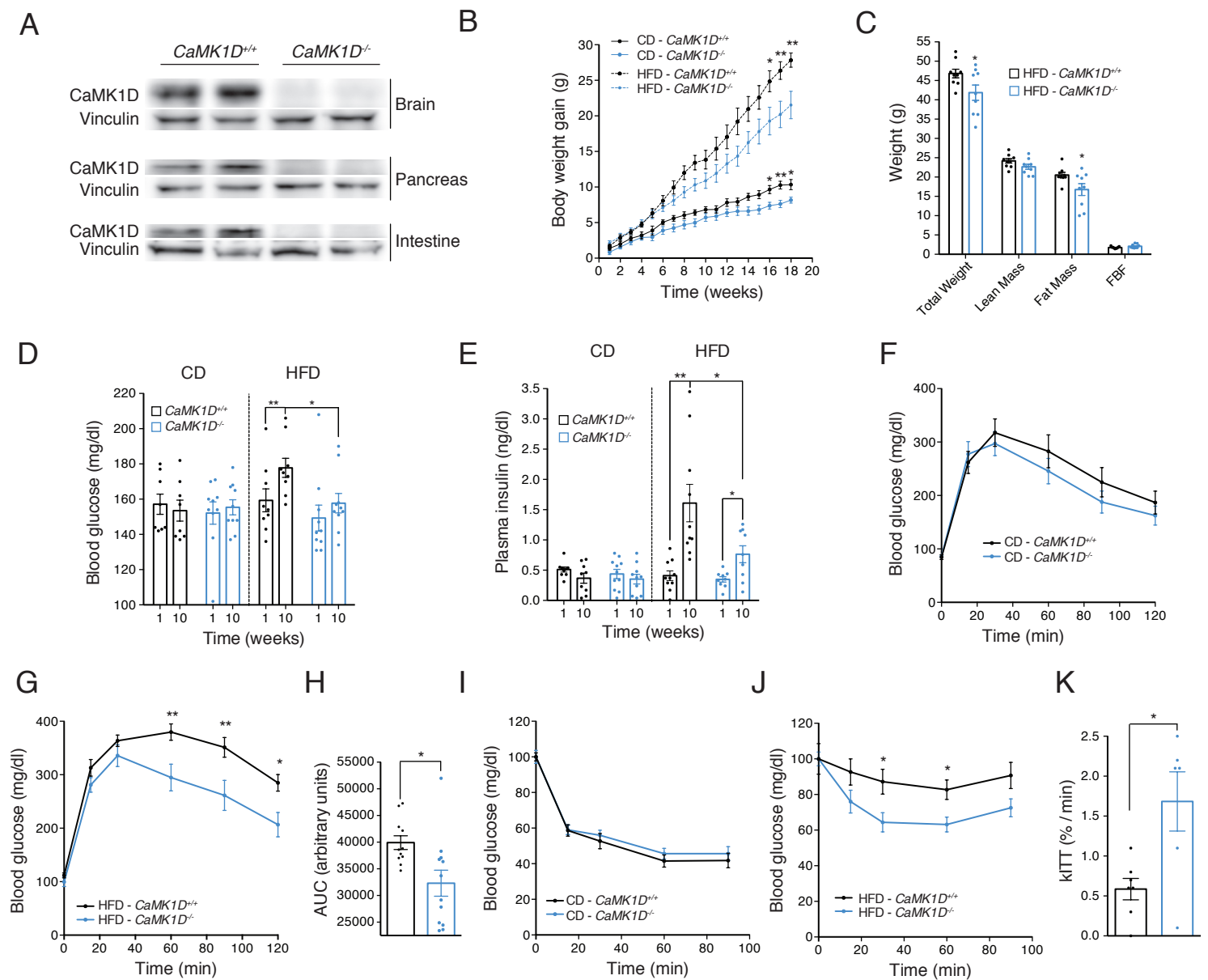


Figure 2

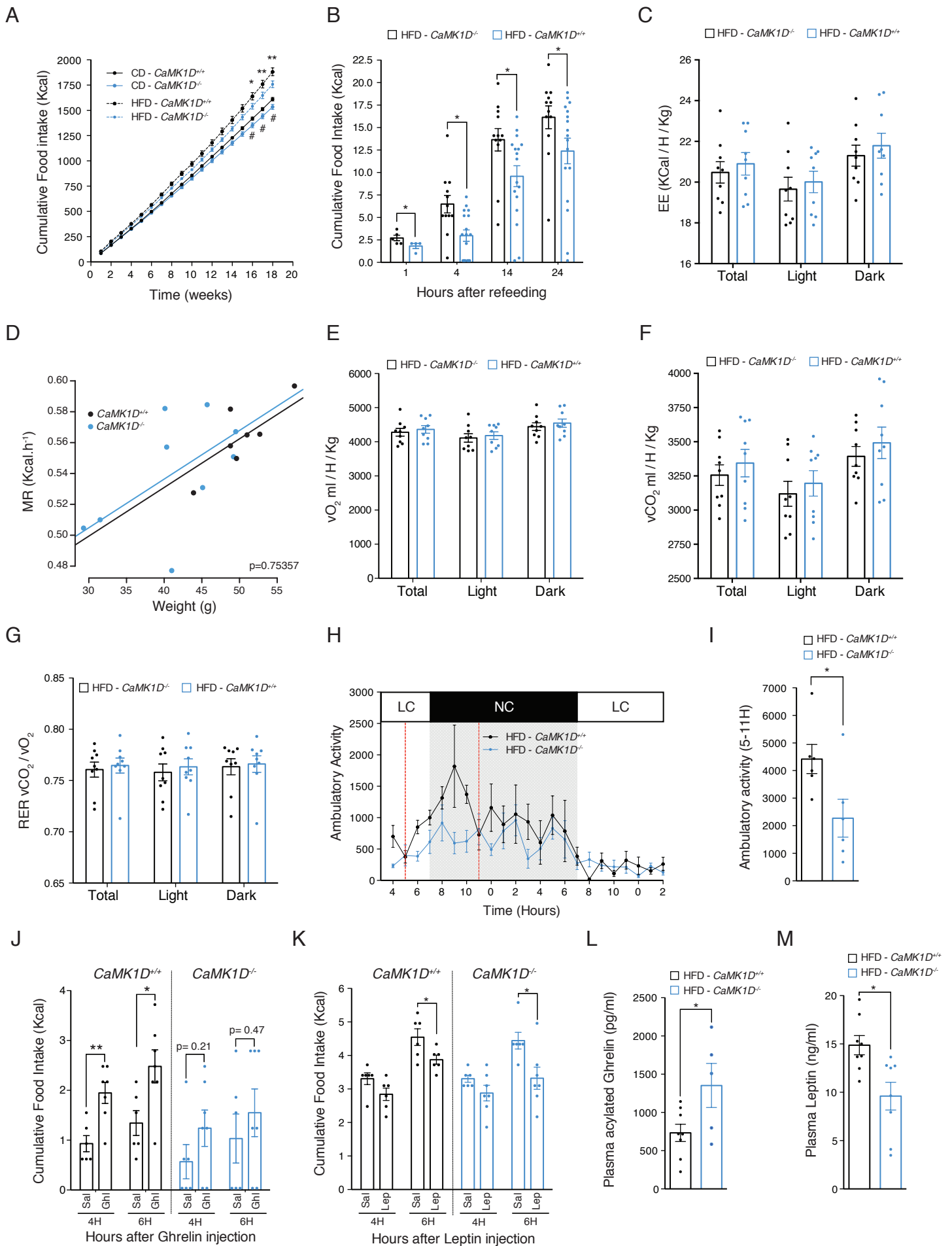


Figure 3

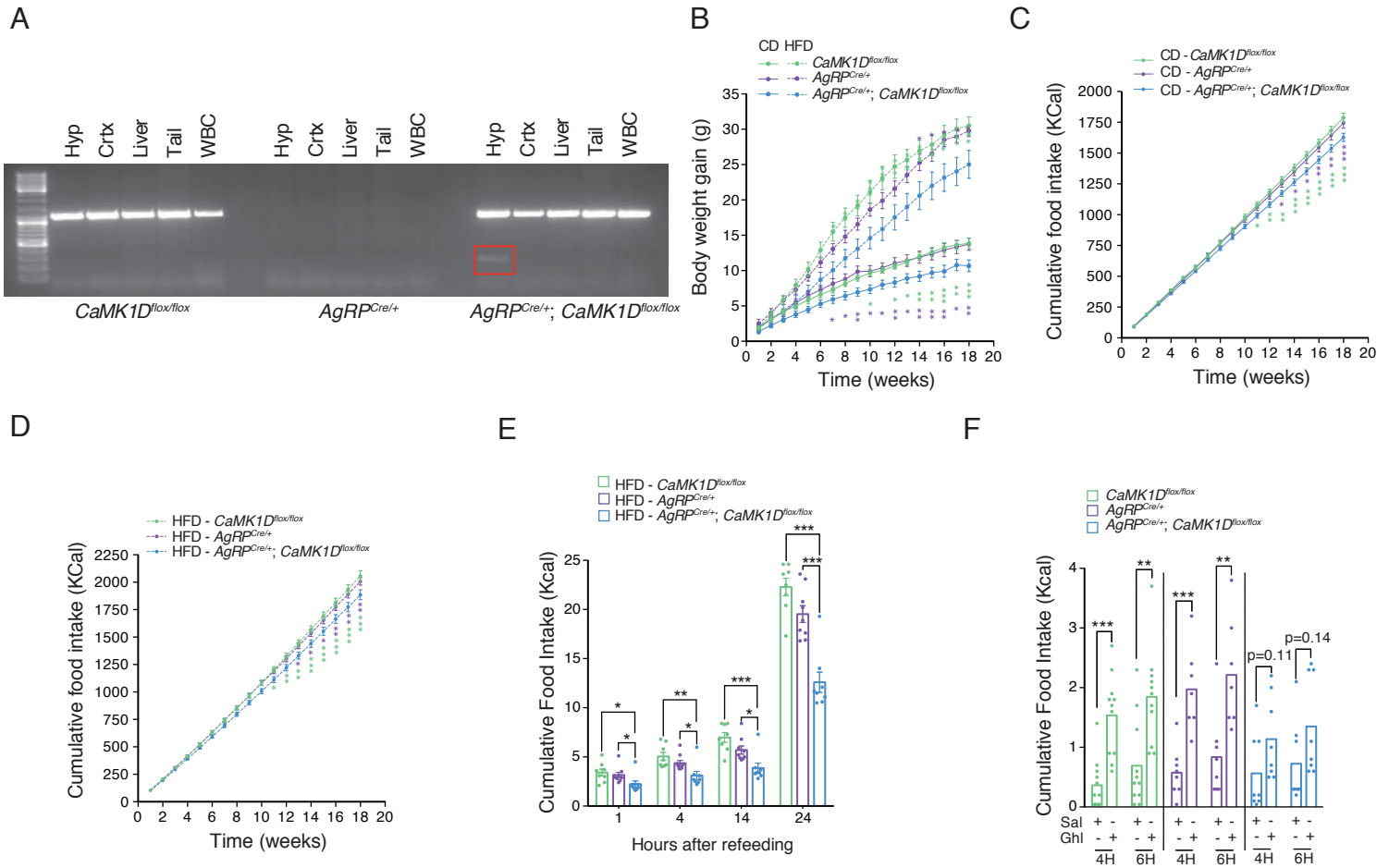
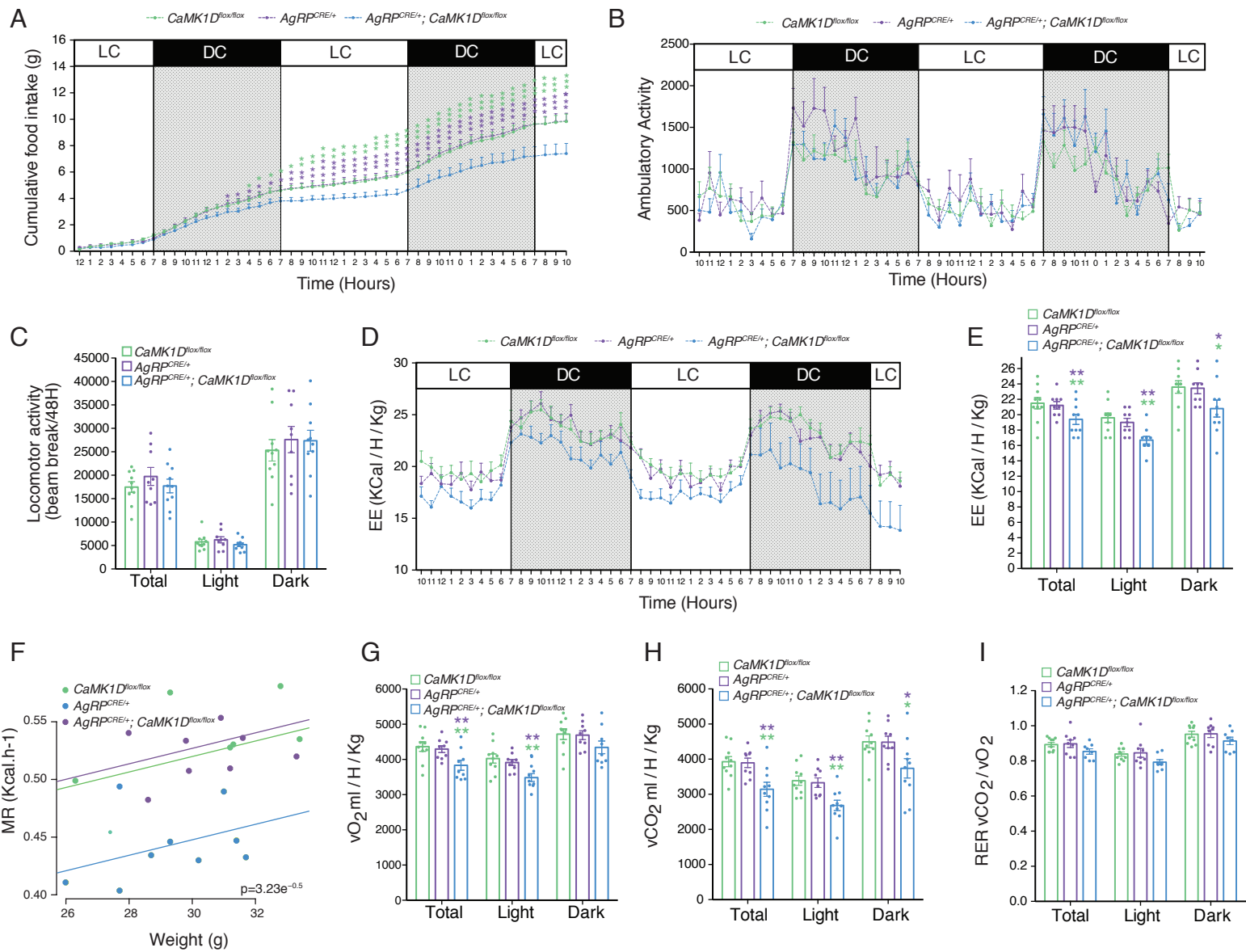
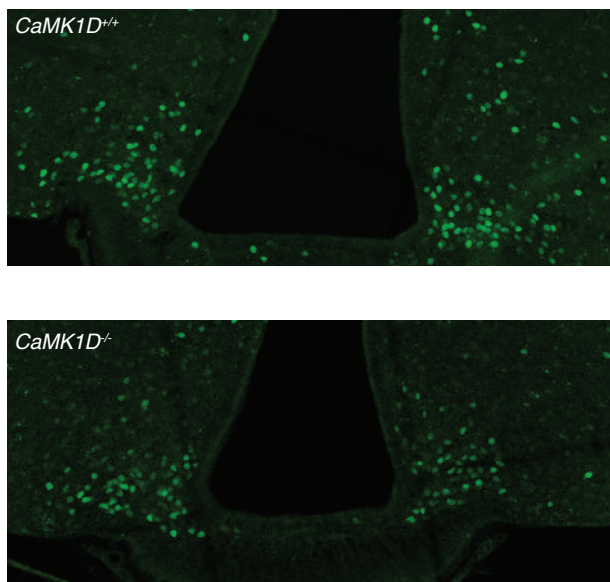


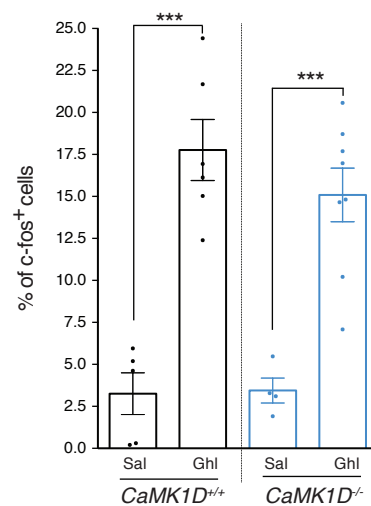
Figure 4



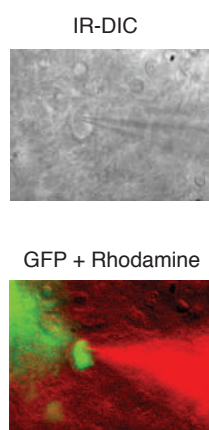
A



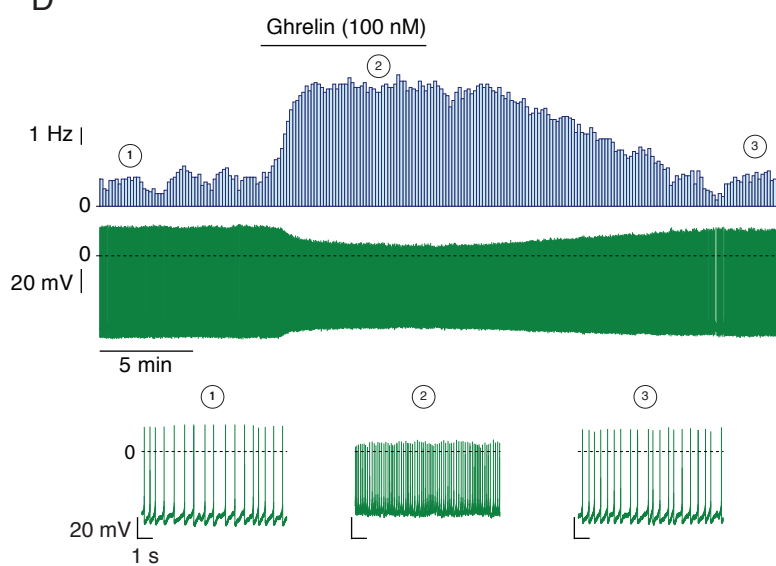
B



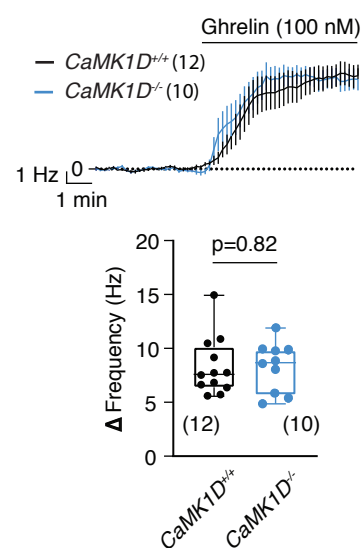
C



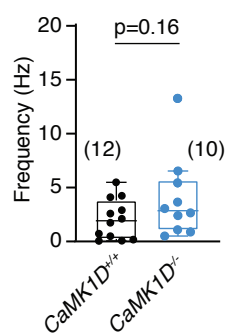
D



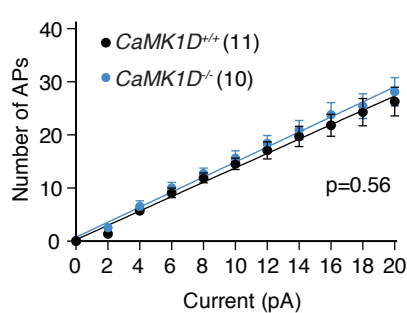
E



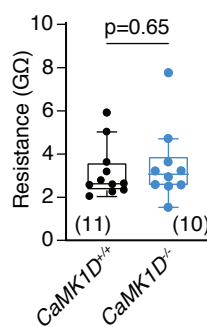
F



G



H



I

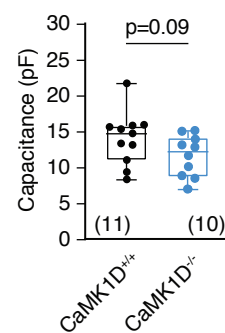


Figure 6

